SIGNAL PROCESSING FOR A PHASE

INTERFEROMETER IN THE PRESENCE OF

MULTIPATH NOISE

by

Kyu San Han

Thesis submitted to the Faculty of the Graduate School
of the University of Maryland in partial fulfilment
of the requirements for the degree of
Master of Science, 1982

ABSTRACT

Title of Thesis: Signal Processing for a Phase Inter-

ferometer in the Presence of Multipath

Noise

Kyu San Han; Master of Science, 1982

Thesis directed by: J.S. Baras
Professor
Department of Electrical Engineering

Direction finding devices, such as phase interfero-
meters, when operating over a rough surface (such as the
sea ocean or terrain) sustain inferior performance. This
performance degradation is due to the so called multipath
interference from reflections by the rough surface. In
this thesis we analyze multipath effects on linear array
phase interferometers. Based on parametric models for
this multipath interference we derive recursive signal
processing algorithms for estimating the angle of arrival
of electromagnetic plane waves. Comparison with other
existing algorithms is also provided.

ACKNOWLEDGEMENT

TABLE OF CONTENTS

1. INTRODUCTION

Direction finding devices such as phase interferometers, when operating over a rough surface (such as the sea ocean or terrain) sustain inferior performance. This performance degradation is due to the so called multipath interference from reflection by the rough surface. In this thesis, we analyze multipath effects on linear array phase interferometers. Considering the underlying parameters in multipath phenomena, we derive recursive signal processing algorithms for estimating the angle of arrival of incident microwave plane waves. Specifically, our approach is a sequential computation of the maximum likelihood estimate of source direction using a bank of Kalman filters operating on the received data. The structure of the thesis is as follows. In Chapter 2, simple models of multipath phenomena are presented in relation with general direction finding problems. The effects of multipath on a horizontal linear array interferometer are qualitatively analyzed also. In Chapter 3, we review the typical approaches to the estimation of the source signal's direction of arrival in linear array interferometers. We present here an extensive literature review including various configurations of interferometer system, assumptions on the observation models, and the resulting estimation schemes. In Chapter 4, we derive the sequential maximum likelihood algorithms for horizontal linear array interferometer. Firstly, a prototype receiver model for pulsed

modulation is described to set nomenclature, specify the interferometer operation and received data and to describe the assumptions used in this work. As mentioned previously, we incorporate multipath phenomenon effects explicitly in the observation model. The so called channel spread function [12] is employed to explain the direction spread in some detail. The problem of estimating the source direction is then formulated as a sequential hypothesis test under certain assumptions. The most critical assumption is a restriction on the source motion. Three versions of the proposed algorithm are then presented, depending on the model of the combined source signal. The problem associated with the measurement of underlying parameters is discussed briefly in connection with state-space models of diffuse multipath component from the rough surface. We carry out the detailed implementation of the proposed algorithm in one example. Recursive equations for estimating the source direction are derived using Kalman filtering. In later section of Chapter 4, we extend the statistic used in Section 3.3 (see [9]) by formulating the problem of ambiguity resolution as sequential hypothesis testing and by combining it with the usual statistic for fine resolution of source direction.

2. MULTIPATH PHENOMENON EFFECTS ON PHASE INTERFEROMETERS

2.1 Basic Interferometer

An elementary interferometer measuring angle of arrival of microwave signals is provided by the simple two element interferometer in Fig. 2.1
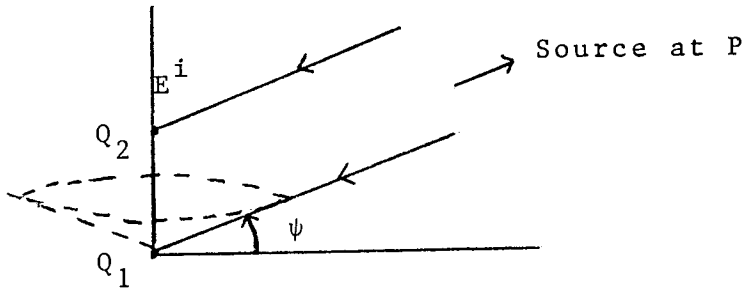

Fig. 2.1. Basic interferometer

Consider a distant source at P radiating a plane wave field that is incident on two identical receiving antennas located at positions Q_1 and Q_2, which are separated by a distance d. The angle of incidence is measured from the normal to the line connecting Q_1 and Q_2. Propagation of the form exp $j(\omega t - kr)$ is assumed, where $k = 2\pi/\lambda$ and λ is the known wavelength. Denoting the incident electric field intensity E_2 at Q_2 by E^i, the field intensity at Q_1 is equal in magnitude to E^i but retarded in phase because of the additional path length.

$$E_2 = E^i$$
$$E_1 = E^i e^{-jk \cdot d \sin \psi}$$
$$\frac{E_2}{E_1} = e^{jk \cdot d \sin \psi} = e^{j\phi_{12}}. \qquad (2.1)$$

Functioning as a direction finding device, angle ψ is obtained from the inverse relation,

3

$$\psi = \sin^{-1}(\frac{\phi_{12}}{kd}).$$

Always the overall antenna separation satisfies $d > \lambda$.

Writing the last relationship in the form

$$\phi_{12} = 2\pi \frac{\sin \psi}{(\frac{1}{d/\lambda})} \qquad (2.2)$$

it may be seen that ψ ranges from $0 \leq \psi \leq \frac{\pi}{2}$, while ϕ_{12}

satisfies $0 \leq \phi_{12} \leq \phi_0$ where $\phi_0 > 2\pi$. ϕ_{12} changes by 2π

rad as $\sin \psi$ increases by factor of $1/(d/\lambda)$. For example,

assume $d = 10\lambda$, then $0 \leq \phi_{12} \leq 20\pi$ as is shown in the

following table.

ψ (degrees)	$\sin \psi$	ϕ_{12} (radians)
0	0	0
5.73	0.1	2π
11.50	0.2	4π
17.50	0.3	6π
$\vdots$		
90	1.0	20π

As the ratio d/λ is made larger, the angle ψ can be

determined with greater precision for given amount of

phase error in ϕ_{12}, provided that the phase ambiguity

explained above is resolved (i.e., the phase angle ϕ_{12} can

be measured uniquely only within 2π rad). Considering a

range of ψ from $-\frac{\pi}{2}$ to $\frac{\pi}{2}$, the usual simple way to overcome

this phase ambiguity is to use $\lambda/2$ spacings between sensors

in the configuration of the array or to employ certain

4

nonuniform spacings such as explained in Section 3.3.

Referring to Fig. 2.1, the angle ψ determines a cone of revolution about the axis of symmetry through Q_1 and Q_2. It is evident that the direction of arrival cannot be determined from measurements with a single axis interferometer. In order to determine the source position P in both azimuth and elevation, two interferometers may be oriented orthogonally as shown in Fig. 2.2. Simultaneous measurements using the x axis interferometer (Q_3, Q_4) and z axis interferometer (Q_1, Q_2) determine the source direction unambiguously by (α, β), since underlined space X is blocked by radiation patterns of antennas and facilities in practice.
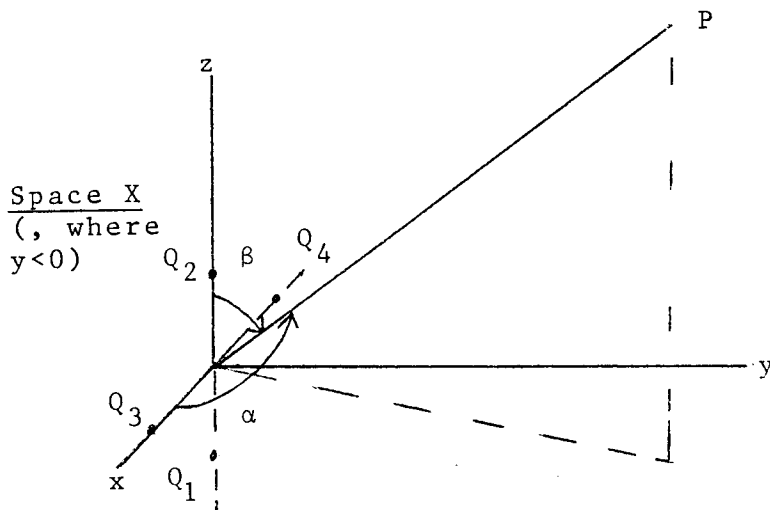
Fig. 2.2. Orthogonal pair of interferometers

2.2 Multipath phenomenon

In real enviroments the signal from an emitter arrives at the antennas through multitudes of indirect

5

paths as well as the direct path, due to scatterings from rough surfaces. Accordingly, any direction estimation system should suffer from the effects of multipath induced direction spread. In this section, we describe briefly some simple characteristics of the scattered field.

It is well known that the observed field, scattered from a rough surface, can be considered as the sume of specular component and diffuse component. This was validated by the analysis of field scattered by a normally distributed surface and also in the investigation of other statistical models of rough surfaces as well as by many experiments [1]. In the sequel, we assume homogeneous rough surface.

Specular component

If considering specular reflection from perfectly smooth surface, the total observed signal voltage is given by (refer to figure 2.3) [1] [2]

$$E = A_t f(\psi_t) + A_r \rho_o \cdot D \cdot f(-\psi) e^{-j\alpha} \qquad (2.3)$$

where A_t and A_r represent the free space field strengths of the direct and reflected field, respectively at the antenna, and $f(\psi_t)$ and $f(\psi)$ are the voltage gains of the atenna along the direct and reflected paths, respectively. D is the divergence factor for curved earth, and ρ_o is the magnitude of the Fresnel reflection coefficient, so that $\rho_o D$ represents the reflection coefficient of smooth but spherical earth. Finally α is the total phase shift of the

reflected field relative to the direct one.

$$\alpha = 2\pi \, \delta_o / \lambda + \phi$$

where δ_o is the extra length of the reflected path and ϕ is the phase angle of the Fresnel reflection coefficient.
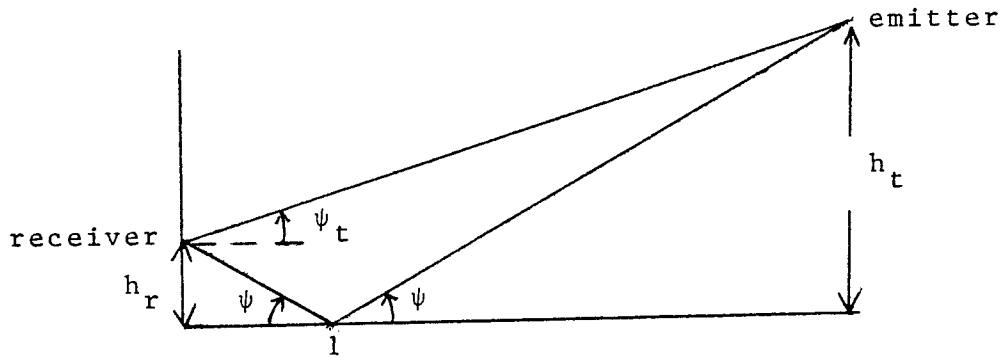

Fig. 2.3. Geometry of specular reflection

To a first approximation, reflected energy originates from the first Fresnel zone [1], defined as the set of the points p on the surface such that $\delta(p) - \delta(I) < \frac{\lambda}{2}$, where $\delta(p)$ is the optical path of a light ray travelling from emitter to receiver by way of reflection at point p. I is the point of reflection, given by the optical specular point.

The effects of the rough surface are accounted for by introducing multiplication of $\rho_o D$ by the complex scattering coefficient ρ_S, the statistics of which depend on the irregularities of the rough surface, with mean square $<\rho_S \rho_S^*>$ showing strong directivity toward specular direction for small irregularities.

Let the surface height $\xi(x,y)$ be distributed normally with mean value $<\xi> = 0$ and standard deviation σ, i.e., let

7

the distribution of ξ be given by

$$w(z) = \frac{1}{\sqrt{2\pi}\ \sigma}\ \exp(-z^2/2\sigma^2) \tag{2.4}$$

The correlation coefficient $C(\tau)$ is assumed to be given by

$$C(\tau) = \frac{<\xi(\vec{r})\xi(\vec{r} + \vec{\tau})>}{<\xi^2(\vec{r})>} = e^{-\tau^2/T^2}; \tag{2.5}$$

T is the characteristic correlation distance, for which $C(\tau)$ drops to e^{-1} isotropically in XY plane. For such a normally distributed surface, the average value of ρ_S in the specular direction, used as the specular reflection coefficient, is given by [1]

$$<\rho_S> = \exp(-\frac{1}{2}\ (\frac{4\pi\sigma\sin\ \psi}{\lambda})^2), \tag{2.6}$$

where ψ is grazing angle of incidence at the specular point (see figure 2.3). Due to the elongation of the first Fresnel zone, Eq. (2.6) will be, in general, only an approximate expression. As $<\rho_S>$ is real, the phase of the specularly reflected field from a rough surface interferes with the direct field as if the reflecting surface were perfectly smooth.

For more general models of rough surfaces, the distribution of ρ_S depends on σ, the root mean square amplitude of surface height. The variance of ρ_S is zero, when $\sigma=0$ and increases with growing $\frac{\sigma\sin\ \psi}{\lambda}$, a scaling parameter called apparent roughness. Coefficient ρ_S becomes Rayleigh amplitude distributed for large apparent roughness, which means that the scattered field from the first Fresnel

8

region becomes part of the diffuse scattered field observed. However, Beard [2] noticed from experimental data analysis that a phase-coherent component still exists for very rough surfaces which indicates that additional factors have to be taken into account when computing the specular component.

In general, ρ_S fluctuates as though it results from the superposition of a constant field and a field with mean zero, whose real and imagainary part are normally distributed with variances S_1 and S_2. Fig. 2.4 illustrates the result of Beard's experiments [2].
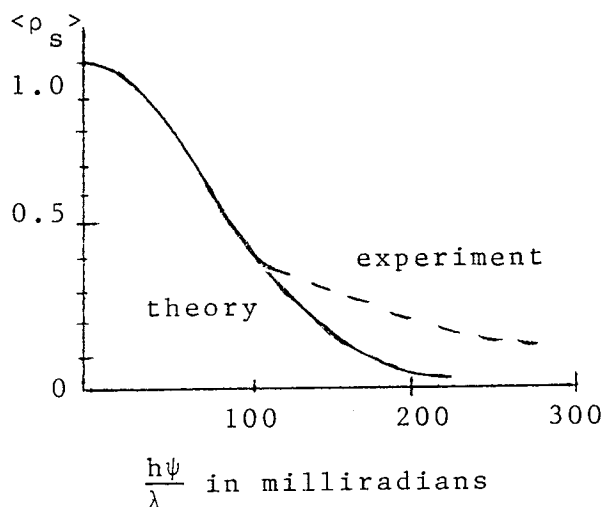
Fig. 2.4. Specular term, theoretical and experimental.

The above experimental results were obtained from L - Q band over the ocean surface. Fresnel reflection coefficient variation with grazing angle is described in F.g 2.5.
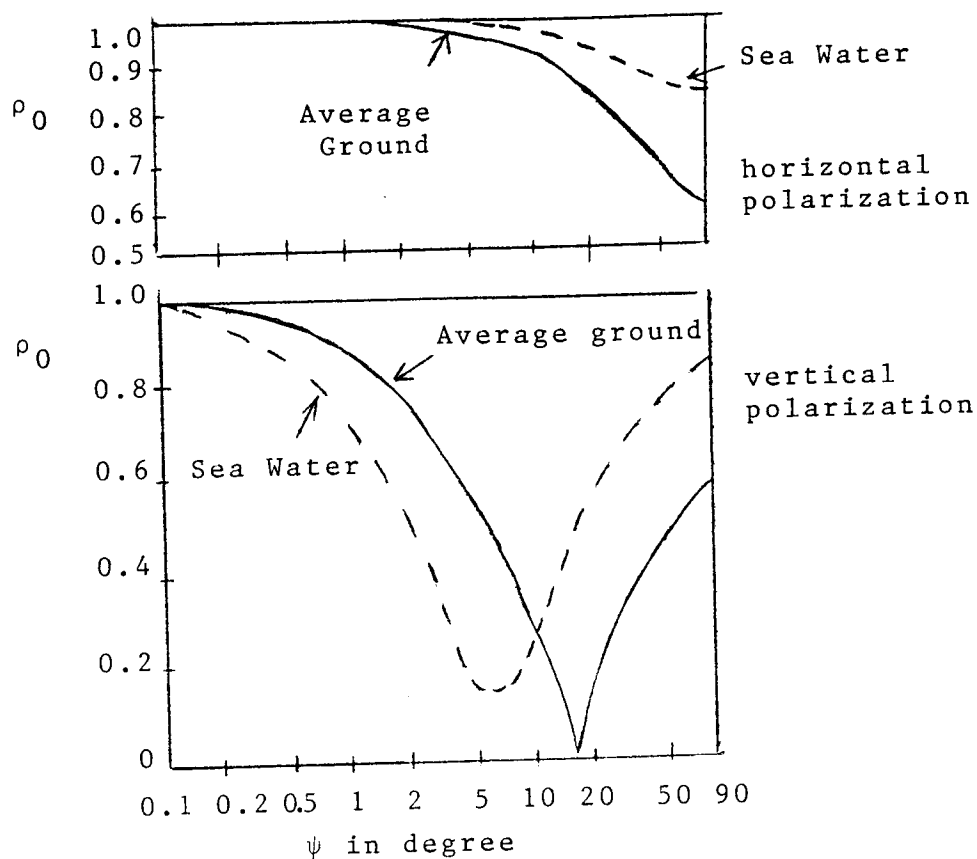
Fig. 2.5. Fresnel reflection coefficient ρ_o for
for horizontal and vertical polarizations, at 1~2GHz

If the surface is covered by vegetation, another
factor, denoted by ρ_v, has to multiply the Fresnel
reflection coefficient ρ_o to account for absorption which
is varying with frequency. In temperate climates, most
of the ground is covered with grass, weeds, trees, bushes,
providing an effective absorbing blanket. Values of ρ_v
between 0.1 and 0.3 are common for microwave frequencies
at grazing angles from 0.5 to 2 degree.

Diffuse component

Diffuse scattering is a phenomenon that has little

10

directivity and which consequently, takes place over a much larger area of the surface than the first Fresnel zone. Its phase is incoherent and its fluctuations are Fayleigh distributed. The following discussion is based on Spizzichino's work [1]. Our objective is to describe a measure of direction spread in the observed diffuse component. The rough surface is modelled as a gaussian surface in the parameter regime $\lambda / \sin \psi < \sigma$. To describe the diffuse field, it is necessary to define the glistening surface S, from where most of the observed diffuse scattered field emanate. Under the above assumption (approximate evaluation of tangent plane method [1]), the expected elemental diffuse power from an elemental area ds on S is given by

$$d\rho_d^2 \cong \frac{ds}{4\pi} \left(\frac{r}{r_1 r_2}\right)^2 \frac{1}{\cos^4\beta} \cot^2\beta_o \exp\left(-\frac{\tan^2\beta}{\tan^2\beta_o}\right) \qquad (2.7)$$

where β is the angle made by the bisector of the incident and scattered rays with the z axis, β_o is given by $\tan\beta_o = \frac{2\sigma}{T}$. The corresponding geometry is described by Fig. 2.6. In (2.7), $d\rho_d^2$ is normalized with respect to the power of direct field. Since the vertical dimension σ (height of the irregularities) is, in most cases, much smaller than the horizontal dimension T (correlation length of the surface), the angle β_o is small. Therefore β is also small since we are interested only for points such that $|\beta| < \beta_o$ (see below for details). Thus (2.7) becomes

$$d\rho_d^2 \cong \frac{1}{4\pi} \left(\frac{r}{r_1 r_2}\right)^2 \cot^2\beta_o \exp\left(-\frac{\tan^2\beta}{\tan^2\beta_o}\right) ds$$

$$\cong \frac{1}{4\pi} \left(\frac{r}{r_1 r_2}\right)^2 \frac{1}{\beta_0^2} \exp\left(-\frac{\beta^2}{\beta_o^2}\right) \cdot ds. \qquad (2.8)$$

From this expression, the bistatic radar cross

section is $\sigma_b = ds/\beta_o^2 \cdot \exp\left(\frac{-\beta^2}{\beta_o^2}\right)$ with reflectivity $\frac{1}{\beta_o}\exp\left(-\frac{\beta^2}{\beta_o^2}\right)$.

Expressions (2.7), (2.8) do not include the effects of

depolarization, shadowing, and multiple scattering. These

factors are important for low grazing angle of incidence

geometries. We will have occasion to refer to T.P.

Mcgarty's calculation [12] in Chapter 4, which consideres

some of these effects. Specular point theory [3] postu-

lates that the observed diffuse field is a superposition

of waves scattered from local specular points whose local

slope is given by β, a tilted angle of local facet. Since

surface slope is normally distributed with standard

deviation $\frac{\beta_o}{\sqrt{2}}$, contributions from points such that $|\beta|<\beta_o$

dominate and this condition is used to define the

glistening surface S (see Figure 2.6). Actually, express-

ion (2.8) provides the pdf of surface slopes, due to the

assumption of $\lambda/\sin \psi<\sigma$.

If antenna gains are considered, the expected elemental

diffuse power, dE_d^2, from ds is given by,

$$dE_d^2 = d\rho_d^2 \cdot E_o^2 \left(\frac{g_1 g_2}{g_{10} g_{20}}\right)^2$$

where,

E_o is the intensity of direct field,

g_{10}, g_1 are the transmitter voltage gains in the direction of the receiver and that of the element ds, respectively,

g_{20}, g_2 are the receiving antenna gains in the same directions

The total ρ_d^2 from the glistening surface S is given by the integral of $d\rho_d^2$ over the glistening surface, using the fact that elemental difuse scattering components add incoherently.

$$\rho_d^2 = \int_S \left(\frac{g_1 g_2}{g_{10} g_{20}}\right)^2 \cdot d\rho_d^2. \qquad (2.9)$$

Consequently, the power coefficient of diffuse scattering Rd is given approximately by,

$$R_d = \rho_d^2 \cdot \rho_o^2$$

where ρ_o is the Fresnel reflection coefficient defined at the specular point on the mean surface. We next consider an example of glistening surface, given by Spizzichino, to describe multipath induced direction spread. The assumption used here is that the heights of transmitting and receiving antennas are small, compared to the distance between them $(h_r, h_t << d)$ and that antenna radiation patterms are isotropic so that the glistening surface is not restricted by antenna patterns. The resulting glistening surface is depicted in figure 2.7 below.
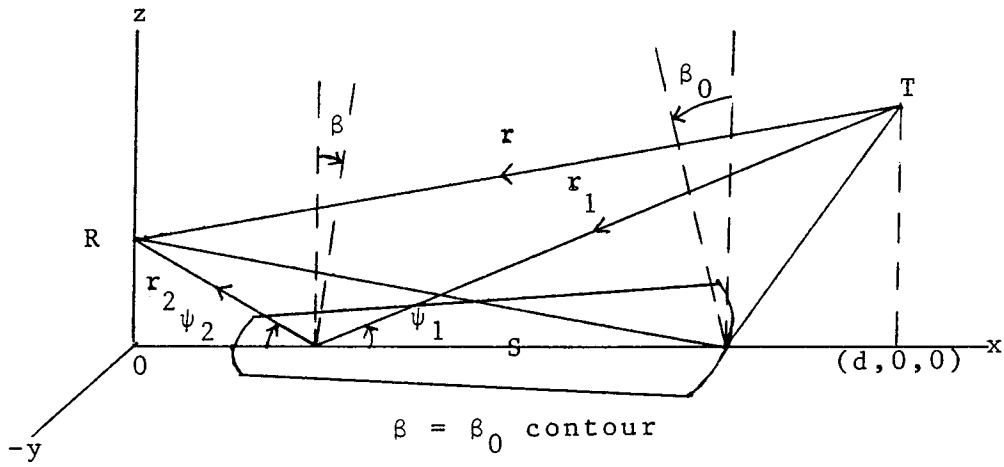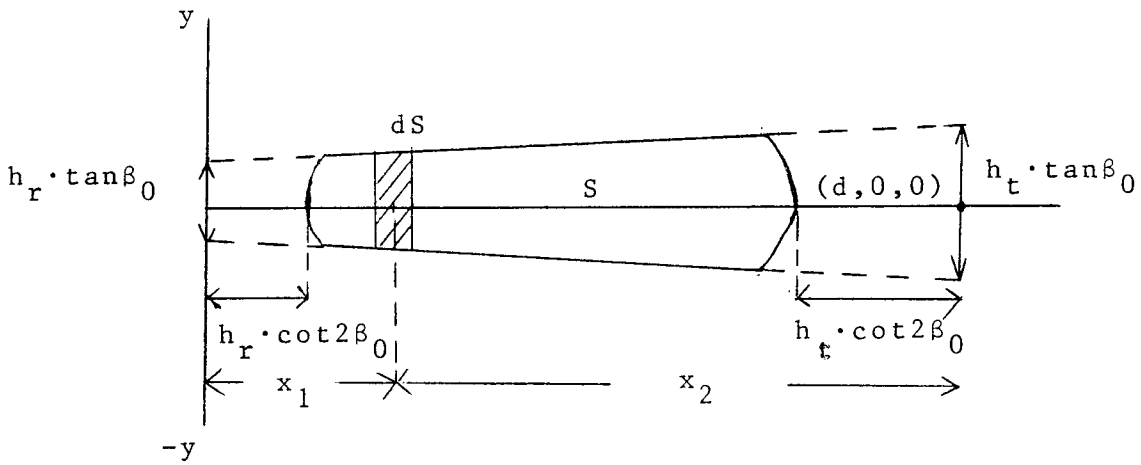
13

Fig. 2.6. The area $\beta \leq \beta_o$.

Fig. 2.7. Glistening surface in example.

The coordinate y of the glistening surface boundary is given by

$$y = \pm \frac{x_1 x_2}{d} \left(\frac{h_r}{x_1} + \frac{h_t}{x_2}\right) \sqrt{\tan^2 \beta_o - \frac{1}{4}\left(\frac{h_r}{x_1} - \frac{h_t}{x_2}\right)^2}. \qquad (2.10)$$

The glistening surface has in general the form of a narrow strip extending along the x axis of the link under the assumption of h_r, $h_t << d$, and can also be used for low angle emitters, for which $h_r << h_t << d$. The power scattering coefficient of an elemental component of the diffuse field, $d\rho_d^2$, can be transformed into elevation power density by taking ds in an approximate way as depicted in Fig. 2.7. We assume $\rho_o^2 = 1$ for all ds' for simplicity and also that β is virtually constant across the y direction of ds with $|\beta| = |\psi_1 - \psi_2|/2$ (see figure 2.6 for definition of ψ_1, ψ_2). Then

$$ds \cong 2 \cdot y_e \cdot dx \cong \sqrt{\pi} \cdot \frac{r_1 r_2}{d} \cdot (\psi_1 + \psi_2) \cdot \beta_o \cdot r_2 \cdot d\psi_2 / \psi_2 \qquad (2.11)$$

$$r_2 d\psi_2 \cong dx \cdot \psi_2$$

where, y_e is the effective width of ds and is given by multiplying y by $\sqrt{\frac{\pi}{4}}$. By combining Eq. (2.8) with Eq. (2.11), and using the approximation $d \cong r$, we obtain

$$d\rho_d^2 = \frac{1}{4\sqrt{\pi}} \cdot \frac{r}{r_1} \cdot (\frac{\psi_1 + \psi_2}{\psi_2}) \cdot \frac{1}{\beta_o} \cdot \exp(-(\frac{|\psi_1 - \psi_2|}{2\beta_o})^2) \cdot d\psi_2$$

$$ = f(\psi_2) d\psi_2. \qquad (2.11)$$

The function $f(\psi_2)$ defines the evevation power density of the observed diffuse field as a function of ψ_2. In azimuth distribution, the azimuth spread at $x_1, \Delta\theta$, is given by,

$$\Delta\theta \cong \frac{\sqrt{\pi} \cdot y}{r_2} = \sqrt{\pi} \cdot \frac{r_1}{r} \cdot (\psi_1 + \psi_2)\beta_o. \qquad (2.12)$$

For a geometry such that $h_r << h_t << d$,
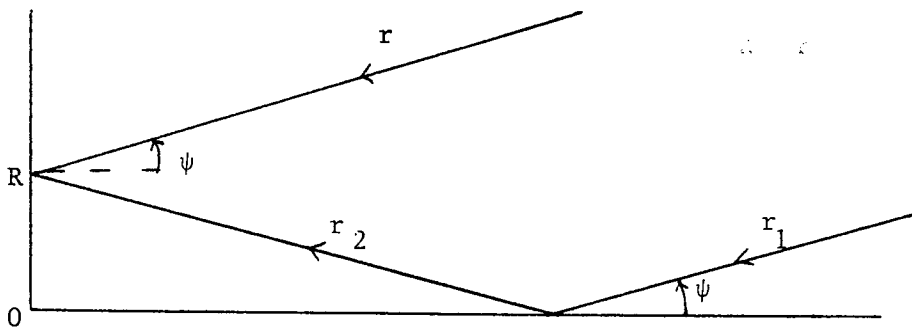
Fig. 2.8

this width becomes $\Delta\theta = 2\sqrt{\pi} \cdot \psi \cdot \beta_o$ near the specular

point, where $r_1 \cong r$, and $\psi_1 = \psi_2 = \psi$. Generally it is

seen that with $\beta_o < 0.1$, azimuth dispersion is quite small

so that diffuse reflections as well as specular ones may

be considered to originate along a line at emitter azimuth

under the specified geometry. Antenna radiation patterns

as well as short pulse duration may also restrict the

surface S where $\beta \leq \beta_o$. Equation (2.8) results in excessive

amount of ρ_d^2, due to the lack of consideration of all the

other factors in scattering. Fig. 2.9 [2] illustrates

experimental results by Beard, performed under similar

conditions as the results described in Fig. 2.4.
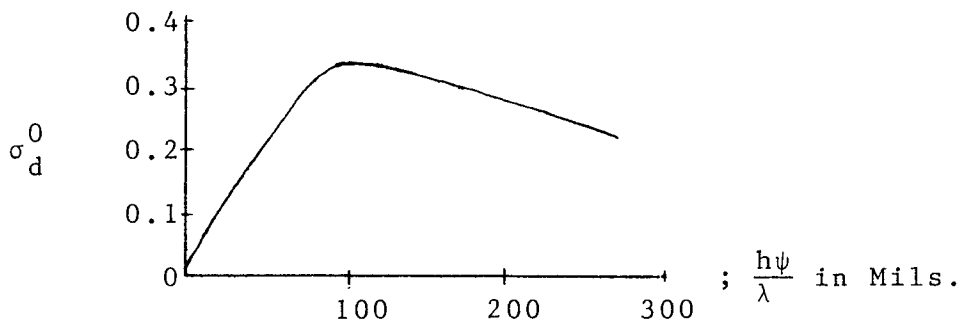
Fig. 2.9. Diffuse field vs apparent ocean roughness.
Incoherent power $= 2(\sigma_d^o)^2 = \rho_d^2$.

16

In addition to the direction spread, the frequency spectrum of the diffuse component is also an important factor in any direction of arrival estimator, since we wish to estimate the performance degradation due to the diffuse component (and therefore modelling of diffuse component is required). Broadening of the spectrum of the diffuse component is known to occur. This result is supported both by theory and experiments. Fig. 2.10 illustrates experimental results by Beard and Katz [4], using X band over ocean surface.
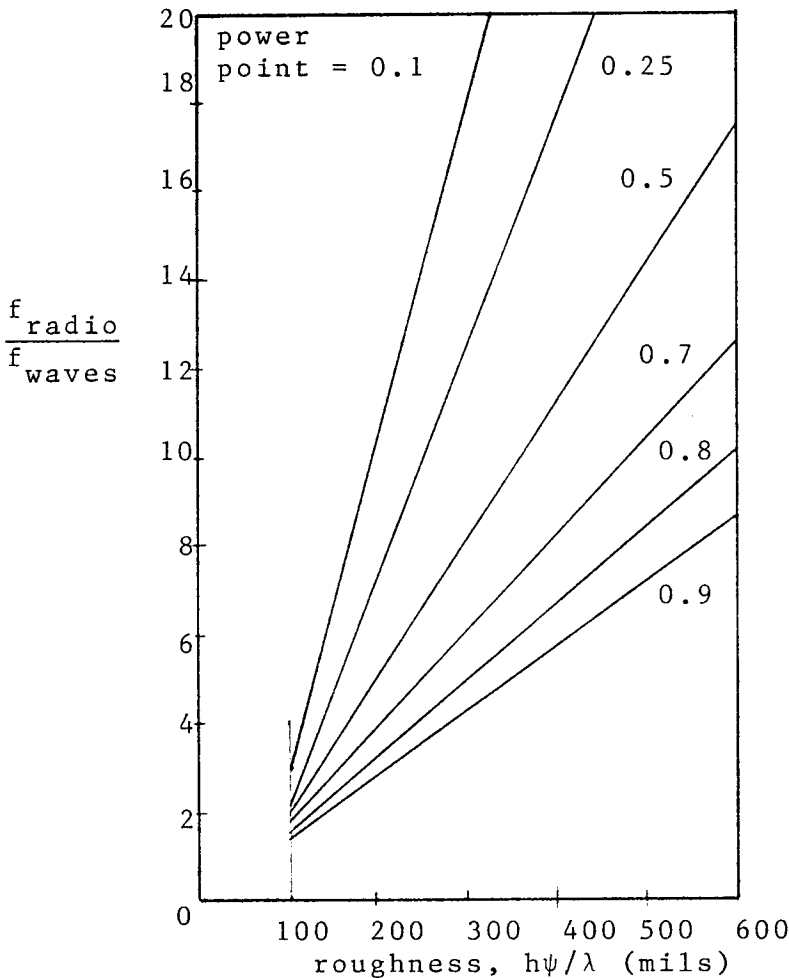
Fig. 2.10. Composite curves of f_{radio}/f_{waves} vs $h\psi/\lambda$ for various power points of diffuse spectra from experimental data.

17

Here, f_{wave} represents maximum frequency of ocean wave
spectrum, $f_r(0.5)$ is the frequency of $\frac{1}{2}$ power point of
diffuse spectra, etc. The reason for the spectrum spread
can be described by the following qualitative argument.
As each small scatterer moves vertically through any height,
it changes its contribution to the phase of the resultant
signal. This phenomenon can be referred to as Doppler
shift with respect to observer. For example, the phase of
the return from a patch near the specular point will vary
as $4\pi(h\psi/\lambda)$ as height h changes, and if it moves through
twice that height in the same time, its contribution to the
frequency of fluctuation is doubled. Thus as wave height
increases, one would expect an increased spectrum bandwidth
generated by harmonics of all the frequencies in the wave
spectrum. In land terrain as well as in ocean surface, as
the emitter moves, the glistening area is changing in time,
which causes fluctuation of observed diffuse component.
Direction spread of diffuse component should account for
spread of pure Doppler shift with respect to direct signal.
Also, the characteristic correlation distance T and thus β_o
as well as the tangential velocity of emitter (with respect
to ground) will affect the spectrum width.

Another important factor to be considered is the
spatial correlation of the diffuse field, since observations
at various points are used in the interferometer array.
However, analytical derivations of spatial correlation is
a rather cumbersome problem and is not addressed here. We

can only state as a general trend, that for gentle slope ($\frac{\sigma}{T}<<1$), surface correlation influences observed field correlation while for steep slopes, emitter-receiver geometry plays a dominant role. Later we will utilize a spatial correlation model defined in a local sense.

We have given a brief description of multipath phenomena. We conclude this section by qualitatively examining the effects of multipath. Direction spread will cause an error in any direction finding system, including interferometers. In the case of the horizontal x axis interferometer in Fig. 2.2, the specular component has some direction cosine, μ_1 (= cos α) as the direct signal for most of geometries of practical interest, so that there is no spread in the direction of arrival. Furthermore, the phase of the specular component associated with each sensor of the array, may well be shifted as in the case of the direct signal (plane wave), as long as the specular component plays a meaningful role (i.e., $\frac{\sigma \sin}{\lambda}<<1$). This can be justified since fluctuations of the specular component are small when $\frac{\sigma \sin \psi}{\lambda}<<1$. Both unspreadness and deterministic phase relationship ensure that the specular component does not cause an appreciable error in horizontal interferometer. However, it causes intensity fluctuations in the observed signal.

On the other hand, the diffuse component, due to its direction spread, will cause errors in the direction estimation. Direction spread of the diffuse component is different than that of plane waves, however. The phase

19

relationship between the set of diffuse components, jointly

observed at the array, is not deterministic as that of

plane waves. This fact as well as the small power level

of the diffuse component (considering homogeneous terrain)

will alleviate the effect of direction spread to some

extent. Finally filtering effects, as the emitter moves

on, are helpful. In Chapter 4, we will treat the hori-

zontal interferometer in detail under the condition that

μ_2 (= cos β) is slowly varying.

3. SURVEY OF TYPICAL ANGLE OF ARRIVAL ESTIMATION SCHEMES

In this chapter, we review previous works related to the angle of arrival estimation in interferometer systems. The maximum likelihood method (ML) is exclusively used in most of these studies. It is characterized by the following properties under reasonably general conditions [5]:

1. The ML estimate converges in probability to the correct value of the parameter, as the number of independent samples goes to infinity. Equivalently, the bias in the ML estimator (if any) diminishes asymptotically.

2. The ML estimate is the efficient estimoator if the latter exists. If not, ML estimate is asymptotically efficient; that is,

$$\lim_{N \to \infty} \frac{\text{Var}[\hat{\theta}_{ML}(\vec{R}) - \theta]}{(-E[\frac{\partial^2 \ell_n p(\vec{R}/\theta)}{\partial \theta^2}])} = 1.$$

where

θ is the unknown parameter to be estimated,

$\vec{R}$ is the N dimensional joint observation,

$p(\vec{R}/\theta)$ is the conditional probability density of $\vec{R}$, given θ,

$\hat{\theta}_{ML}(\vec{R})$ is the ML estimate of θ, given $\vec{R}$,

and also

Var, E denotes variance and expectation respectively, with respect to $\vec{R}$, given θ.

3. The ML estimate is asymptotically gaussian,

$N(\theta, \sigma_{\theta\epsilon})$, where $\sigma_{\theta\epsilon}$ is a variance of the ML

estimate at θ.

The literature reviews given here, emphasizes descriptions

of system condifuration, signal models, and resulting

statistic.

3.1. Case I [6]

The system used here is a minor variation of the basic

variable baseline correlation interferometer, which

employs relative phase detectors between a reference

sensor and the kth sensor of array. Before proceeding,

the configuration of the relative phase detector is shown

in Fig. 3.1.

$$R(t)\cos(\omega t + \phi_R(t); \text{reference}$$

$V(t)\cos(\omega t+\phi(t))$

$\otimes$; multiplier
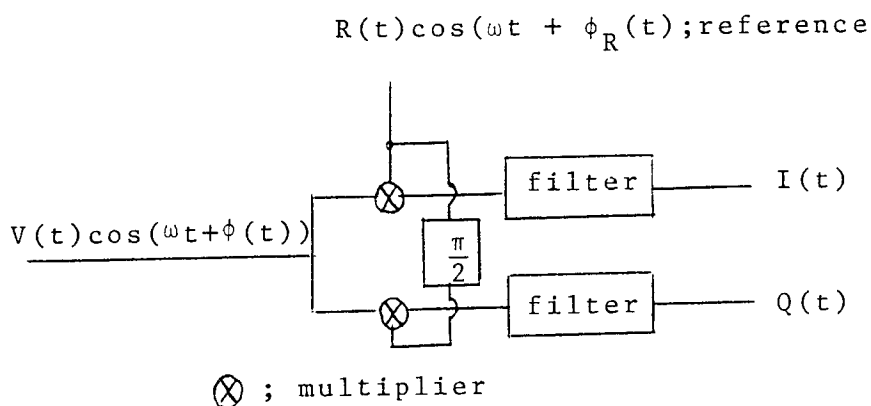
Fig. 3.1. Basic relative phase detector.

$V(t)$, $I(t)$, $\phi(t)$, $\phi_R(t)$ are narrow band-limited signals.

$$I(t) = V(t)R(t)\cos(\phi(t) - \phi_R(t)) \qquad (3.1)$$

$$Q(t) = V(t)R(t)\sin(\phi(t) - \phi_R(t));$$

Here, the constant gain factor is omitted. This relative

phase detector provides quadratures of incoming signal

with respect to reference signal, and thus is used as the

basic block in interferometer systems.

Fig. 3.2 shows the case of the kth baseline pair where the signal is received by the isotropic antennas at A and B separated by k half wavelengths. Half wavelength spacings in this array configuration are taken primarily for simplicity and also to avoid the inherent ambiguity involved in observables; that is, the phase ambiguity. Phase ambiguity will be discussed in more detail in Section 3.3.

Fig. 3.2. Interferometer at k[th] baseline.

Remote noisy point source at angle θ measured from the baseline is exciting the system. The path difference of the source's incoming wave will cause an RF phase difference of $(\frac{2\pi}{\lambda})\ [k(\frac{\lambda}{2})\ \cos\theta] = k\pi\ \cos\theta = k\delta$, where $\delta = \pi\ 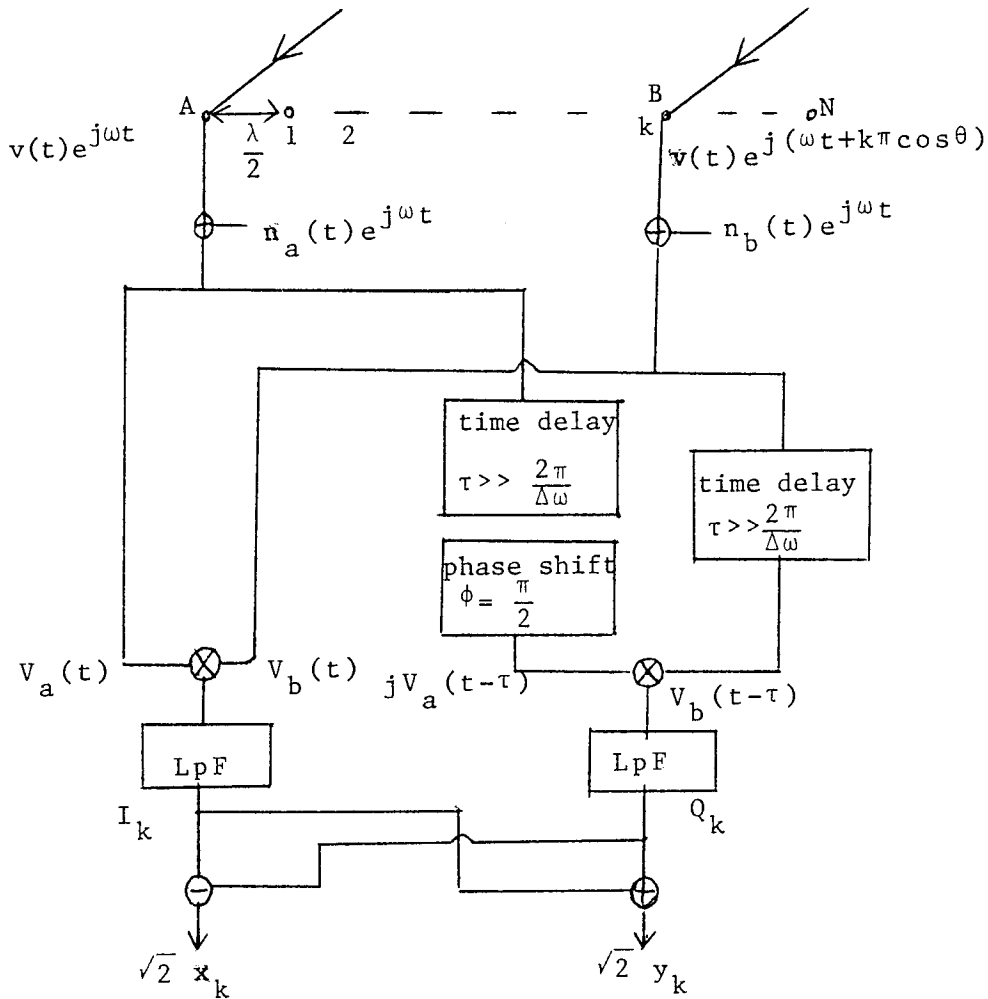\cos\theta\ (-\pi \leq \delta \leq \pi)$. From now on, δ is considered as the direction parameter. According to Fig. 3.2, the kth baseline output is given by,

$$I_k(t) = \text{Re} < V_a(t) V_b^*(t) >\tau_e \qquad\qquad (3.2)$$

$$Q_k(t) = \text{Re} < jVa(t-\tau) \cdot V_b^*(t-\tau) >\tau_e$$

where Re stands for "real part" and $<\cdot>$ for finite averaging process of LP filter. Subscript τ_e represents effective averaging time; that is, the time constant of the low pass filter. Equation (3.2) is, in essence, the same as Equation (3.1), except that complex envelope representation is used, and the bandwidth of LP filter is considered.

It is assumed that the signal

$$v(t) = v'(t) + jv''(t)$$

and noise $\qquad\qquad\qquad\qquad\qquad\qquad\qquad (3.3)$

$$n_a(t) = n_a'(t) + jn_a''(t)$$

$$n_b(t) = n_b'(t) + jn_b''(t)$$

are independent complex gaussian processes, whose quadrature components v', n_a', n_b', etc., have zero means and variances V, N, N, etc., respectively, with flat power spectra within the system bandwidth of Δw rad/s.

$$E\{v^p v^q\} = V\delta_{p,q} \tag{3.4}$$

$$E\{n_\alpha^p n_\beta^q\} = N\delta_{p,q} \delta_{\alpha,\beta}$$

where $p,q \equiv ',"$, $\alpha,\beta = a,b$ and $\delta_{p,q}$, $\delta_{\alpha,\beta}$ are the Kronecker deltas. The noise considered is combination of receiver noise and incoherent background noise uniformly distributed over the angle.

In the ideal case of infinite correlation time (i.e., $\tau_e = \infty$), the filter outputs are the two dc values. Under the assumption of ergodicity $E\{\cdot\}$ is replaced by $<\cdot>_{\tau e=\infty}$.

$$I_k\big|_{\tau e=\infty} = T \cos k\delta, \quad Q_k\big|_{\tau e=\infty} = T \sin k\delta \tag{3.5}$$

Where $T = 2V$ is the total power in the received signal and is proportional to the source strength. However, for a practical averager, the pair I_k, Q_k will be slowly varying random processes whose pdf can be assumed to be gaussian with mean given by Eqs. (3.5), respectively, provided that $\tau_e >> 1/\Delta\omega$. In general I_k is correlated with Q_k, with correlation coefficient $\rho(I_k, Q_k)$ dependent on the delay time τ through the transfer function of the low pass filter. The variances of I_k, Q_k depend on the direction to be estimated. By choosing delay time $\tau > 5\tau e$, I_k, Q_k become virtually decorrelated.

A transformation is performed to obtain the final observables $\{x_k, y_k\}$, whose variances are independent of the parameter δ to be estimated;

$$\begin{bmatrix} x_k \\ y_k \end{bmatrix} = \frac{1}{\sqrt{2}} \begin{bmatrix} 1 & -1 \\ 1 & 1 \end{bmatrix} \cdot \begin{bmatrix} I_K \\ Q_K \end{bmatrix}$$

25

$$E\{x_k\} = T \cos(k\delta + \frac{\pi}{4})$$

$$E\{y_k\} = T \sin(k\delta + \frac{\pi}{4}) \qquad\qquad (3.6)$$

$$\rho(x_k, y_k) = 0.$$

$$\text{Var}\{x_k\} = \text{Var}\{y_k\} = b(T + 2N)^2 = \sigma^2;$$

where b is determined from system parameters. The ratio T/σ (and not T/N) is recognized as the baseline measurement's voltage SNR. Taking sequential samplings of (x_k, y_k), the resulting set of measurements are statistically independent.

With this system configuration the problem is to estimate (T, δ) jointly, given $(x_1, y_1, \ldots, x_N, y_N)$. The conditional pdf of observables, given (δ, T) is,

$$\prod_{k=1}^{N} f_k(x_k, y_k; \delta, T)$$

$$= L(\delta, T; \vec{x}, \vec{y})$$

$$= (2\pi\sigma^2)^{-N} \cdot \exp\{-1/2\sigma^2 \cdot \sum_{k=1}^{N} [(x_k - T \cos \alpha_k)^2 +$$

$$(y_k - T \sin \alpha_k)^2]\}$$

$$\alpha_k = k\delta + \frac{\pi}{4}, \quad k = 1, 2, \ldots, N \qquad\qquad (3.7)$$

The ML estimates $\hat{\delta}$ and $\hat{T}$ jointly maximize L or its logarithm; thus,

$$\left. \frac{\partial}{\partial \delta} \ln[L(\delta, T, x, y)] \right|_{\substack{\delta = \hat{\delta} \\ T = \hat{T}}} = 0 \qquad\qquad (3.8)$$

$$\left. \frac{\partial}{\partial T} \ln[L(\delta, T, \vec{x}, \vec{y})] \right|_{\substack{\delta = \hat{\delta} \\ T = \hat{T}}} = 0$$

Equations (3.7), (3.8) determine the ML processor. The likelihood function $L(\delta, T, \vec{x}, \vec{y})$ has N local maxima with

26

one global maximum, along δ. The Cramer-Rao lower bounds
of estimation errors are computed by taking the diagonals
of Γ^{-1}, where Γ is Fisher's information matrix.

$$\Gamma = E \begin{bmatrix} -\dfrac{\partial^2(\ell_n L)}{\partial \delta^2} & -\dfrac{\partial^2(\ell_n L)}{\partial \delta \partial T} \\ -\dfrac{\partial^2(\ell n L)}{\partial T \partial \delta} & -\dfrac{\partial^2(\ell_n L)}{\partial T^2} \end{bmatrix}$$

$$\sigma_\delta^2 = \frac{\sigma^2}{T^2} \frac{6}{2N^3 + 3N^2 + N} \qquad\qquad (3.9)$$

$$\sigma_T^2 = \frac{\sigma^2}{1 + 4b} \frac{1}{N} .$$

In this referenced paper, results show that the asymptotic
property of ML estimate is achieved with relatively small
N, which is a decreasing function of output SNR.

3.2. Case II [7]

An array of receiving elements is placed in a medium
in which plane waves are incident upon it. Each receiving
element is assumed to have an omnidirectional characteristic.
The geometry of the array is shown in Fig. 3.3. An
arbitrary coordinate system is placed at the center of the
array and the position of the ith receiving element is
given by the displacement (d_i) along the x-axis. A plane
wave whose propagation vector is lying in the XY plane, is
incident on the array at an angle θ.

27
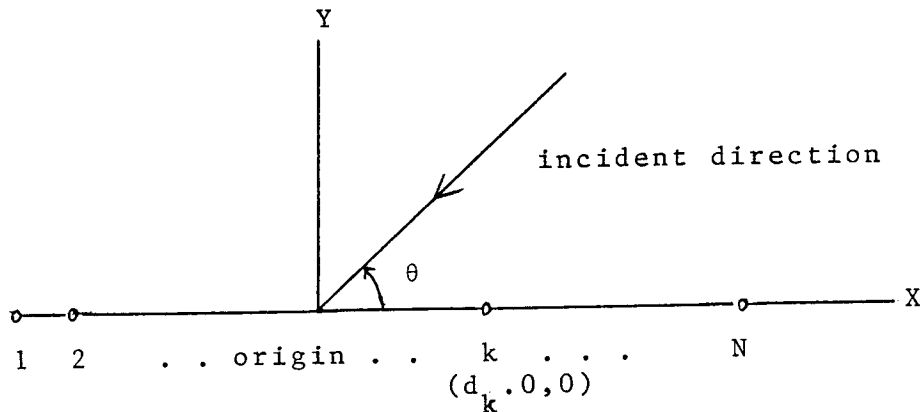
Fig. 3.3. Interferometer array geometry

Here, the XY plane is the plane formed by the incident ray and the axis of array. The array actually measures polar angle relative to its axis, considering phase shift relationship between sensors. At any position vector $\vec{r}$, the plane wave may be represented by the form $A_o \exp[j(-\vec{k} \cdot \vec{r} + \phi + \omega t)]$, where A_o is the amplitude, $\vec{k}$ is the propagation vector, ω is the angular frequency, and ϕ is an arbitrary phase. ϕ is assumed to be uniformly distributed on $(0, 2\pi)$ and independent of A_o, and A_o is assumed to be Rayleigh distributed with known variance. This model implies that in-phase and quadrature components of the signal have gaussian amplitude. In complex signal notation, the output signal from the kth sensor is then given by,

$$\tilde{b} \sqrt{\frac{\overline{E_s}}{T}} \exp(j \, 2\pi(\frac{d_k}{\lambda}) \cos\theta + j\omega t), \qquad (3.10)$$

where, $\tilde{b}$ is a complex gaussian random variable with zero mean and

28

$$E(\tilde{b}\tilde{b}*) = 2 \cdot \sigma_b^2 \qquad\qquad (3.11)$$

The term $(E_s/T)^{1/2}$ is a normalization term, where E_s is defined as the undisturbed signal energy and T is an observation interval. At each sensor, we also observe noise $\tilde{n}_k(t)$, which is assumed to be narrowband, zero mean, complex gaussian noise. Therefore, in complex notation, the narrowband output of the kth sensor, $\tilde{r}_k(t)$, is given by,

$$\tilde{r}_k(t) = \tilde{b}(\frac{E_s}{T})^{1/2} \exp(j\ 2\pi\frac{d_k}{\lambda}\mu) + \tilde{n}_k(t), \qquad (3.12)$$

where μ is the direction cosine, $\cos\theta$. As a convention taken in this reference, the observed output $r_k(t)$ equals $\sqrt{2}\ \text{Re}[\tilde{r}_k(t)\ \exp(j\omega t)]$. Provisions are made to measure the inphase and quadrature components $\tilde{r}_k(t)$, at the output of kth sensor.

The complete observation is represented by the N sensor outputs and this can be compactly written in vector notation as

$$\vec{r}(t) = \tilde{b}[\frac{E_s}{T}]^{1/2}\ \vec{m}(\mu) + \vec{n}(t) \qquad\qquad (3.13)$$

where, $\vec{\tilde{r}}(t)$ is the Nx1 vector with components $\tilde{r}_k(t)$ and

$$\vec{m} = \begin{bmatrix} \exp(j2\pi\frac{d_1}{\lambda}\mu) \\ \vdots \\ \exp(j2\pi\frac{d_N}{\lambda}\mu) \end{bmatrix} \qquad\qquad (3.14)$$

The observation variable $\vec{\tilde{r}}$ for signal processing is defined

by

$$\vec{r} \triangleq \int_0^T \frac{1}{\sqrt{T}} \vec{r}(t) dt$$

$$= \int_0^T \frac{1}{\sqrt{T}} \{ \tilde{b} [\frac{E_s}{T}]^{1/2} \vec{m}(\mu) + \vec{n}(t) \} dt$$

$$= \tilde{b} \cdot \vec{s} + \vec{N} \qquad (3.15)$$

with $\vec{N} = \frac{1}{\sqrt{T}} \int_0^T \vec{n}(t) dt,$

where $\vec{s}$ equals $\sqrt{E_s} \vec{m}(\mu)$ and $\vec{N}$ is a zero-mean complex

gaussian vector with covariance matrix $2 \cdot K_N$. $\tilde{b}$ is assumed

to be constant during the observation period T.

$$E(\vec{N} \vec{N}^+) = 2 \cdot K_N \qquad (3.16)$$

where "+" denotes complex conjugate transpose. The ML

estimate μ, given $\vec{r}$ is given by generating two dummy hypo-

theses, H_0 and H_1. Under H_1, $\vec{r}$ is given by (3.15) and

under H_0, $\vec{r}$ is just $\vec{N}$.

$$L(\vec{r}, \mu) \triangleq \frac{p(\vec{r}/H_1, \mu)}{p(\vec{r}/H_0)}$$

$$= \frac{E_{\tilde{b}} [p(\vec{r}/H_1, \mu, \tilde{b})]}{p(\vec{r}/H_0)}; \qquad (3.17)$$

where $E_{\tilde{b}}$ denotes expectation with respect to $\tilde{b}$.

We can proceed directly, based on (3.17). However, we

will take a more general approach [8]. Under hypothesis

$H_1, \mu,$

$$\vec{r}(\mu) = \tilde{b}\vec{s}(\mu) + \vec{N} = \vec{z}(\mu) + \vec{N}$$

Let $2 \cdot K_r^\mu = E(\vec{r}(\mu) \vec{r}^+(\mu))$

$$= E(\vec{z} \, \vec{z}^+) + E(\vec{N} \, \vec{N}^+)$$

$$= 2 \cdot K_z^\mu + 2 \cdot K_N \qquad (3.18)$$

$$p(\vec{r}/H_1, \mu) = (\frac{1}{\pi})^N \cdot \frac{1}{|2K_r^\mu|} \cdot \exp\{-\vec{r}^+ (2 \cdot K_r^\mu)^{-1} \vec{r}\}$$

$$\qquad (3.19)$$

$$p(\vec{r}/H_o) = (\frac{1}{\pi})^N \cdot \frac{1}{|2K_N|} \cdot \exp\{-\vec{r}^+ (2 \cdot K_N)^{-1} \vec{r}\}.$$

Given $\vec{r}$, the minimum mean square error estimate of $\vec{z}$,

denoted by $\vec{z}_e$, is given by

$$\vec{z}_e = H\vec{r}(\mu); \text{ where H is the (N,N) matrix}$$

$$H = 2 \cdot K_z^\mu (2 \cdot K_r^\mu)^{-1}$$

$$= K_z^\mu \cdot (K_r^\mu)^{-1}$$

$$= (K_r^\mu - K_N)(K_r^\mu)^{-1} = I - K_N (K_r^\mu)^{-1}. \qquad (3.20)$$

Multiplying both sides of equation (3.20) on the left

by K_N^{-1} gives,

$$(K_r^\mu)^{-1} = K_N^{-1} - K_N^{-1} H. \qquad (3.21)$$

Combining (3.19) with (3.20), (3.21) gives

$$L(\vec{r}, \mu) = \frac{p(\vec{r}/H_1, \mu)}{p(\vec{r}/H_o)}$$

$$= \frac{|K_N|}{|K_r^\mu|} \cdot \exp(\frac{1}{2} \vec{r}^+ K_N^{-1} \cdot H \cdot \vec{r})$$

$$= \frac{|K_N|}{|K_r^\mu|} \cdot \exp(\frac{1}{2} \vec{r}^+ K_N^{-1} K_z^\mu \cdot (K_r)^{-1} \cdot \vec{r}). \qquad (3.22)$$

But $K_z^\mu = \sigma_b^2 \, \vec{s} \, \vec{s}^+(\mu)$

$$K_r^\mu = \sigma_b^2 \, \vec{s} \, \vec{s}^+(\mu) + K_N \qquad (3.23)$$

31

Substituting (3.23) into (3.22), and manipulating matrices, we have

$$L(\vec{r}, \mu) = \frac{\sigma_T^2}{\sigma_b^2} \{ \frac{1}{2} \cdot \sigma_T^2 \cdot \vec{r}^+ K_N^{-1} \vec{s} \ \vec{s}^+ K_N^{-1} \vec{r} \} \tag{3.24}$$

where

$$\sigma_T^2 = \frac{\sigma_b^2}{1 + \sigma_b^2 \vec{s}^+ K_N^{-1} \vec{s}} . \tag{3.25}$$

The maximum likelihood estimate of μ, $\hat{\mu}$ is obtained by measuring $\vec{r}$ and using it in (3.24), and then finding the μ that maximizes that expression. Also (3.24) can be used for detection purposes with some preset Λ_o. The likelihood ratio in (3.24) has another interpretation as an estimator correlator, as is clear from (3.20).

$$\hat{\tilde{b}} = \sigma_T^2 \vec{s}^+ K_N^{-1} \vec{r} \tag{3.26}$$

where $\hat{\tilde{b}}$ is MMSE estimate under hypothesis H_1, μ, given $\vec{r}$. Thus (3.24) can be written as,

$$L(\vec{r}, \mu) = \frac{\sigma_T^2}{\sigma_b^2} \exp(\frac{1}{2} \vec{r}^+ K_N^{-1} \hat{\tilde{b}} \ \vec{s}) . \tag{3.27}$$

This is the estimator correlator form for the likelihood ratio. This is also further simplified by noting that K_N^{-1} can be written as $W^+ W$ where W is a whitening matrix. Then, defining $\vec{s}_w$ as $W\vec{s}$ and $\vec{r}_w$ as $W\vec{r}$, we have

$$L(\vec{r}, \mu) \approx \frac{\sigma_T^2}{\sigma_b^2} (\frac{\hat{\tilde{b}}}{2} \vec{r}_w^+ \ \vec{s}_w(\mu)) . \tag{3.28}$$

A processor implementing this result, is shown in Fig. (3.4).
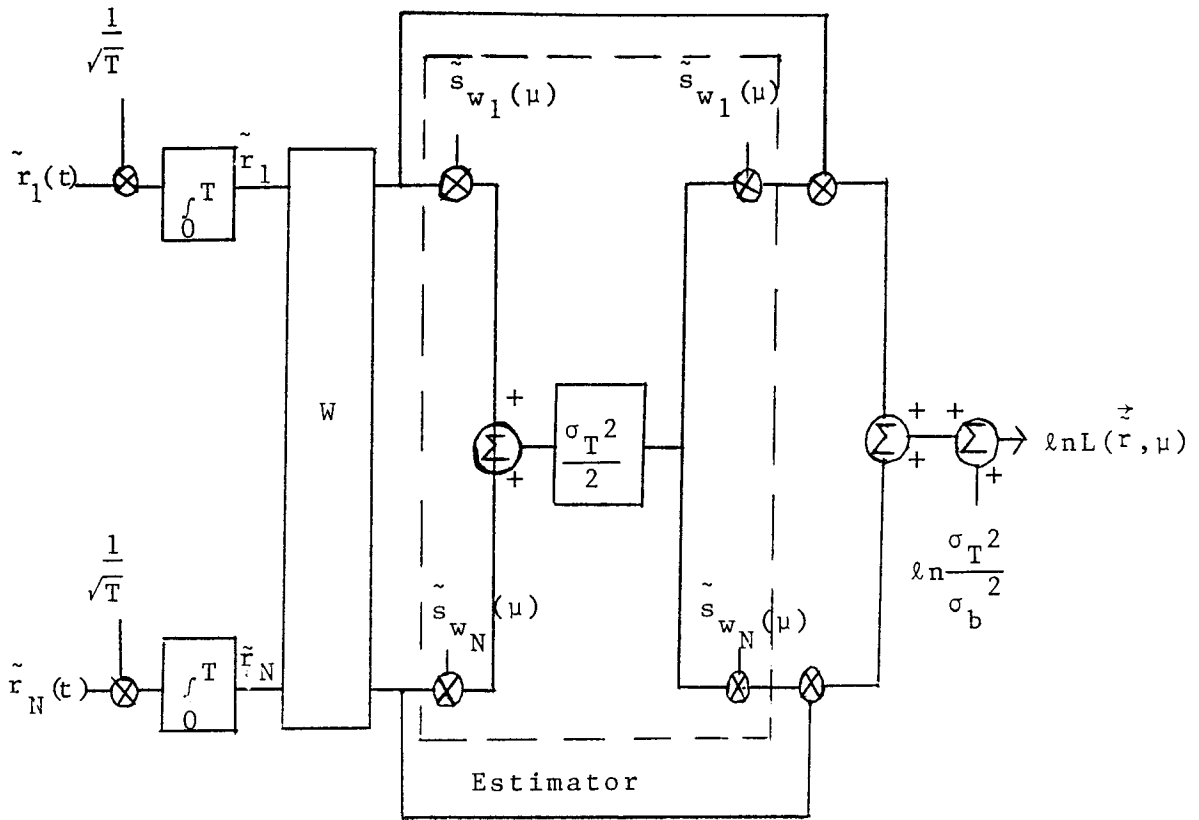
Fig. 3.4. Estimator-Correlator receiver.

Specifically, considering the case when K_N equals $\frac{N_o}{2} I$,
the likelihood ratio (3.24) becomes,

$$L(\vec{r},\mu) = \frac{\frac{N_o}{2}}{(\frac{N_o}{2}) + N\sigma_b^2} \cdot \exp[\frac{1}{2} \frac{\sigma_b^2}{\frac{N_o}{2}(N\sigma_b^2 + \frac{N_o}{2})} |\vec{r} + \vec{s}|^2] \qquad (3.29)$$

When the array is uniformly distributed with spacing d_o,
the Cramer-Rao lower bound is,

33

$$\text{var}(\mu - \hat{\mu}) \geq -\frac{1}{E[\frac{\partial^2}{\partial\mu^2}\ell_n L(\vec{r},\mu)]}$$

$$= \frac{12}{(\frac{2\pi d_o}{\lambda})\left[\frac{E_s\sigma_b^2}{N}\right]} \cdot \frac{1}{(N^3 - N)} \cdot \{1 + \frac{\frac{N_o}{2}}{NE_s\sigma_b^2}\} \tag{3.30}$$

3.3. Case III. [9]

In this reference, a 3 element linear interferometer with nonuniform spacings is used. Depending on the location of the reference sensor, two types of configurations are possible.
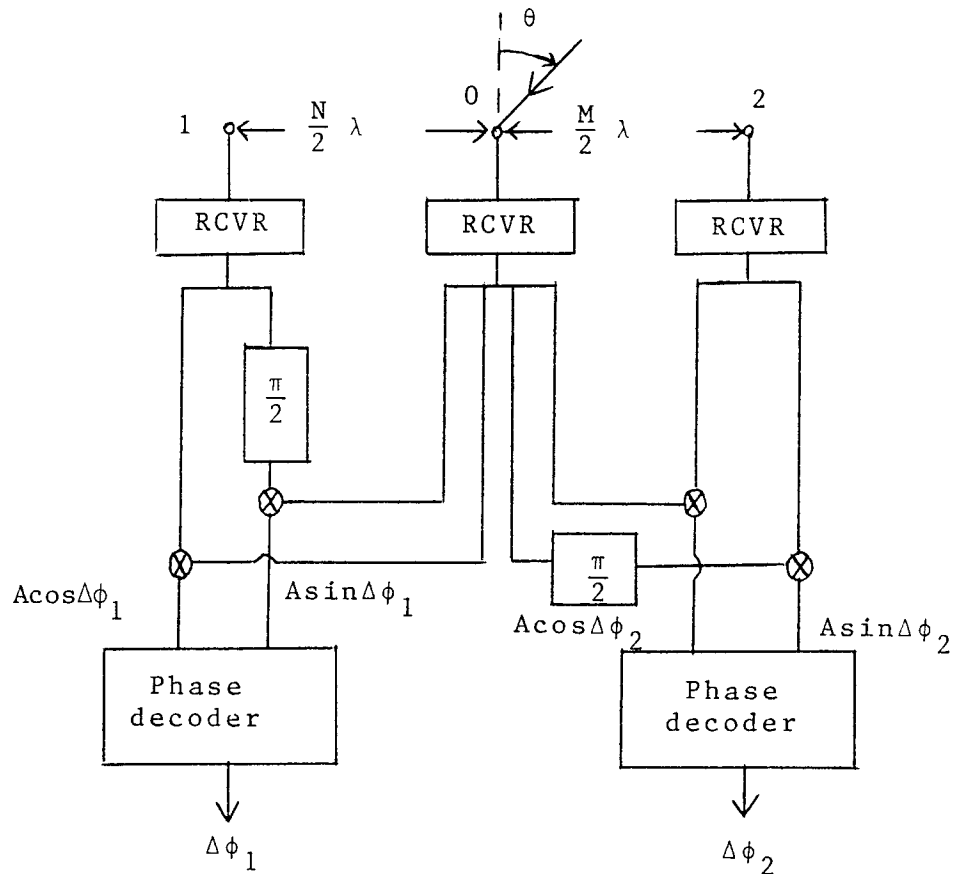
Fig. 3.5. Midphase Configuration.
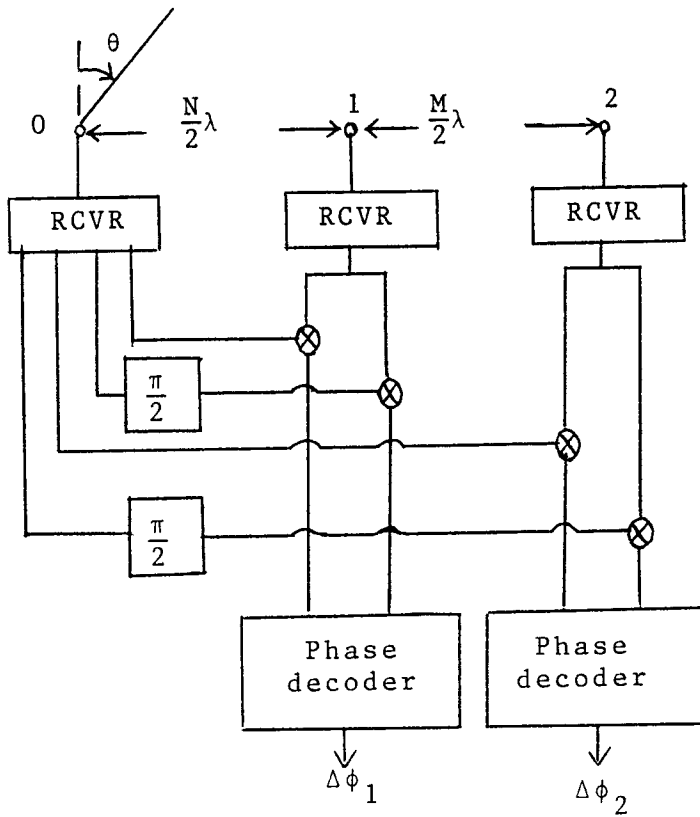
Fig. 3.6. End phase configuration.

Figures 3.5 and 3.6 show block diagrams of the Mid and End phase three elements interferometer systems. Signals from a linear array of three antennas are passed through narrow band receivers and one signal is correlated with quadrature components of the other two to produce measurement proportional to the sine and cosine of the phase differences, $\Delta\phi_1$ and $\Delta\phi_2$. If the emitter is located somewhere in the far field region at an angle θ from the normal to the array axis, the resultant phase differences will be given by:

35

<center>Mid phase case</center>

$$\Delta\phi_{1m} = [N\pi \sin \theta] \text{ Modulo } 2\pi = \phi_o - \phi_1$$

$$\Delta\phi_{2m} = [M\pi \sin \theta] \text{ Modulo } 2\pi = \phi_2 - \phi_o$$

<center>End phase case</center>

$$\Delta\phi_{1e} = [N\pi \sin \theta] \text{ Modulo } 2\pi = \phi_1 - \phi_o$$

$$\Delta\phi_{2e} = [(M + N)\pi \sin \theta] \text{ Modulo } 2\pi = \phi_2 - \phi_o$$

where N, M are the inter-sensor spacings in units of half wavelengths. Modulo 2π means that observed phase is modulo 2π of absolute phase. Thus, the phase difference between a pair of sensors separated by $D \cdot \frac{\lambda}{2}$ is one-to-one mapping of θ only for θ in $[-\sin^{-1} 1/D, \sin^{-1} 1/D)$; $|D \cdot \pi \cdot \sin| < \pi$, to avoid phase ambiguity.

Lemma.

When two colinear sensor pairs with separations of D_1 and D_2 half wavelengths are used, mapping from θ into $(\Delta\phi_1, \Delta\phi_2)$ plane is one to one for θ restricted to $\theta \in (-\sin^{-1} 1/g, \sin^{-1} 1/g)$.

Here, D_1, D_2 are integers greater than or equal to one

g = greatest common divisor of D_1 and D_2.

Proof.

Let $D_1 = g \cdot d_1$, $D_2 = g \cdot d_2$. Assume $D_2 > D_1$. Assume θ_1 and θ_2 are in the range of $(-\sin^{-1} 1/g, \sin^{-1} 1/g)$. Observation set, $(\Delta\phi_1^1, \Delta\phi_2^1)$ is defined as the phase differences due to θ_1. Likewise $(\Delta\phi_1^2, \Delta\phi_2^2)$ is defined as those due to θ_2.

<center>36</center>

Also assume $\theta_2 > \theta_1$. Suppose $(\Delta\phi_1^1, \Delta\phi_2^1) = (\Delta\phi_1^2, \Delta\phi_2^2)$.
Since $\theta_2 > \theta_1$, the only way these two observations are the same should be given from phase ambiguity.

$$g \cdot d_1 \cdot \pi \cdot \sin\theta_2 - g \cdot d_1 \cdot \pi \sin\theta_1 = 2n_1\pi \quad (n_1 \geq 1)$$

$$\tag{3.31}$$

$$g \cdot d_2 \cdot \pi \cdot \sin\theta_2 - g \cdot d_2 \cdot \pi \cdot \sin\theta_1 = 2n_2\pi \quad (n_2 \geq 1).$$

Thus $n_1 = n_2 \cdot \dfrac{d_1}{d_2}$. Substituting $n_2 = k_2 \cdot d_2 + \ell \; (\ell < d_2)$ gives $n_1 = k_2 \cdot d_1 + \dfrac{d_1}{d_2} \cdot \ell$.

Since (d_1, d_2) is a coprime pair, ℓ should be zero for n_1 to be an integer. Thus,

$$n_1 = k_2 \cdot d_1 \text{ and } k_2 \geq 1 \tag{3.32}$$

From (3.31), $\sin\theta_2 - \sin\theta_1 = \dfrac{2 \cdot n_1}{g \cdot d_1}$. From (3.32) $\sin\theta_2 - \sin\theta_1 = \dfrac{2 \cdot k_2}{g} \geq \dfrac{2}{g}$.

Contradiction results, since both θ_1 and θ_2 lie in the range of $(-\sin^{-1} 1/g, \sin^{-1} 1/g)$. Hence $<\Delta\phi_1^1, \Delta\phi_2^1> \neq <\Delta\phi_1^2, \Delta\phi_2^2>$ for $\theta_1, \theta_2 \epsilon (-\sin^{-1} 1/g, \sin^{-1} 1/g)$.

Thus, for D_1, D_2 relatively prime integers, the relation between θ and $(\Delta\phi_1, \Delta\phi_2)$ is one-to-ine for $|\theta| < \dfrac{\pi}{2}$ regardless of magnitudes of D_1, D_2.

Therefore, given observation set $(\Delta\phi_1, \Delta\phi_2)$ can be processed to recover the correct value of θ in the absense of noise. The important aspects of the θ estimation process are well illustrated by the so-called ambiguity diagram, shown in Fig. 3.7 for the case of a Midphase interferometer with spacings of 3 and 4 half wavelengths.
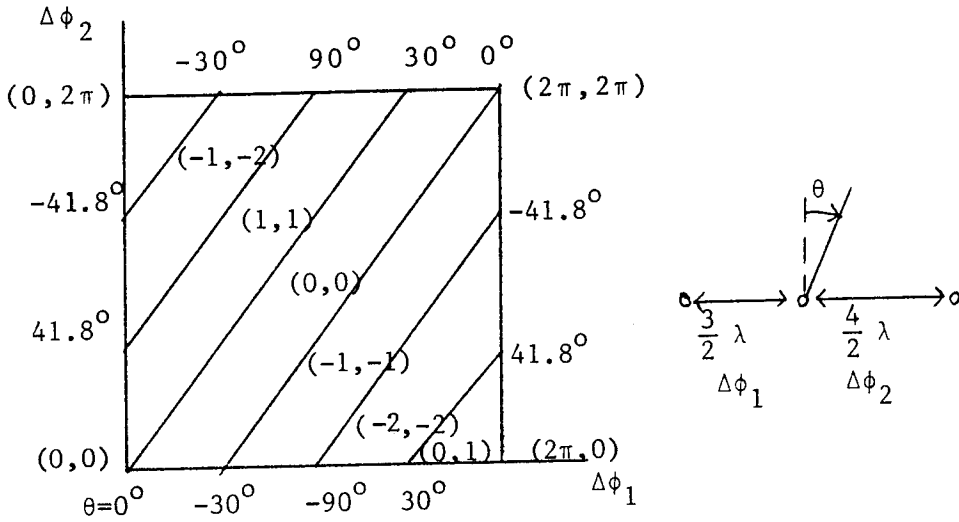
Fig. 3.7. Ambiguity diagram.

In Fig. 3.7, $\Delta\phi_1 = 3\pi \sin\theta - 2k_1\pi$, $\Delta\phi_2 = 4\pi \sin\theta - 2k_2\pi \cdot (\cdot,\cdot)$ represents $(k_1 \cdot k_2)$. The principal phase plane is taken as $(2\pi \times 2\pi)$.

As shown on the figure, the set of points corresponding to all possible noiseless measurements form parallel straight lines of slope, 4/3 in this case. When additive noise is present on the two measurements, the measured point is displaced from the solid lines, and estimation procedure is to obtain estimate $\sin\hat\theta$ from $(\Delta\phi_1, \Delta\phi_2)$.

In terms of the ambiguity diagram, estimation procedure will first determine probable set of (n_1, n_2) and then estimate $\sin\theta$ as a whole. The two parts of the estimation may be viewed as ambiguity resolution and fine resolution.

The result of the ambiguity resolution will either be correct or incorrect, and if it is incorrect, the resultant effect on the angle estimate will be in error by such a

38

large amount that the exact value of the error is of relatively little importance. Such errors are referred to as gross errors for this reason. It is the probability that gross errors will occur that is important as a system performance measure. The error in the fine resolution, since it can take on an uncountable number of values, will be nonzero with probability 1, so that variance is a measure of performance.

Let's proceed to the statistical assumptions of observables, the relative phase differences. The phase measurements made by the interferometer system will, in general, be in error, due to noise present in the system and its environment. This noise, being narrow band, can be represented by the quadrature components with respect to some arbitrary phase reference ϕ_o,

$$n(t) = m^1(\phi_o, t)\cos(\omega t + \phi_o) + m^2(\phi_o, t)\sin(\omega t + \phi_o),$$

where m^1, m^2 are real independent gaussian signals, and are written as functions of ϕ_o to emphasize that another choice of phase reference would result in different samples of m^1, m^2. The statistical properties of m^1, m^2, however, are independent of ϕ_o, making the choice of representation one of convenience.

Composite signal plus noise is,

$$s(t) + n(t) = A\cos(\omega t + \phi_o) + m^1(t)\cos(\omega t + \phi_o)$$
$$+ m^2(t)\sin(\omega t + \phi_o) \qquad (3.33)$$

The resultant phase is then,

39

$$\phi_o - \phi_\epsilon = \phi_o - \tan^{-1}\left[\frac{m^2}{A + m^1}\right].$$

Let the variance of m^1, m^2 be σ_o^2 respectively, also assume that σ_o^2 is independent of θ. For SNR of interest, $A^2/\sigma_o^2 \geq 10$, it is shown that approximation below holds.

$$\tan^{-1}\frac{m^2}{A + m^1} \cong \frac{m^2}{A + m^1} \cong \frac{m^2}{A} \triangleq z.$$

Consequently, probability density function of phase error ϕ_ϵ approximates gaussian distribution

$$p(z) = \frac{A}{\sqrt{2\pi}\,\sigma_o}\exp\left[\frac{-A^2 z^2}{2\,\sigma_o^2}\right]. \tag{3.34}$$

Having established statistics for phase error in model (3.33), statistics of observables in each of two configuration follows immediately. For Midphase configuration of Fig. 3.5,

$$\phi_o = \phi_o^o - \frac{m_o^2}{A} \quad;\text{ phase disturbed at reference sensor}$$

$$\phi_1 = \phi_1^o - \frac{m_1^2}{A} \quad;\text{ phase disturbed at 1st sensor}$$

$$\phi_2 = \phi_1^o - \frac{m_2^2}{A} \quad;\text{ phase disturbed at 2nd sensor.}$$

Further assumption is such that $m_p^i(t)$'s are independent with each other.

The measured phase differences can be written as,

40

$$\Delta\phi_1 = [\phi_0 - \phi_1] \text{ Modulo } 2\pi$$

$$= (\phi_0^0 - \phi_1^0) + \frac{1}{A}(-m_0^2 + m_1^2) - 2\pi k_1$$

$$= p\pi \sin\theta + \Delta\phi_\epsilon^1 - 2\pi k_1$$

$$\Delta\phi_2 = [\phi_2 - \phi_0] \text{ Modulo } 2\pi \qquad\qquad (3.35)$$

$$= (\phi_2^0 - \phi_0^0) + \frac{1}{A}(-m_2^2 + m_0^2) - 2\pi k_2$$

$$= q\pi \sin\theta + \Delta\phi_\epsilon^2 - 2\pi k_2$$

where p,q = baseline lengths in half wavelengths.

$$k_1 = \text{integer part of } (p\pi \sin\theta + \Delta\phi_\epsilon^1)/2\pi$$

$$k_2 = \text{integer part of } (q\pi \sin\theta + \Delta\phi_\epsilon^2)/2\pi.$$

Treating (k_1, k_2) as parameters, covariance matrix of $(\Delta\phi_1, \Delta\phi_2)$ is

$$P \triangleq \text{Cov}(\Delta\phi_1, \Delta\phi_2)$$

$$= E(\Delta\phi_\epsilon^1, \Delta\phi_\epsilon^2)^T (\Delta\phi_\epsilon^1, \Delta\phi_\epsilon^2)$$

$$= \begin{bmatrix} 2 & -1 \\ -1 & 2 \end{bmatrix} \sigma^2 \qquad\qquad (3.36)$$

where $\sigma^2 = \sigma_0^2/A^2$.

For End phase configuration of Fig. 3.6,

$$\Delta\phi_1 = p\pi \sin\theta + \frac{1}{A}(m_0^2 - m_1^2) - 2\pi k_1$$

$$\Delta\phi_2 = q\pi \sin\theta + \frac{1}{A}(m_0^2 - m_2^2) - 2\pi k_2.$$

Corresponding covariance matrix is given as,

$$P = \begin{bmatrix} 2 & 1 \\ 1 & 2 \end{bmatrix} \sigma^2 \qquad .$$

Now, ML estimate can be derived, based on the observation model described so far. Conditional pdf for observation set $(\Delta\phi_1, \Delta\phi_2)$ is,

$$p(\Delta\phi_1, \Delta\phi_2 / \sin\theta, k_1, k_2)$$

$$= \frac{1}{2\pi|P|^{1/2}} \exp\left[-\frac{1}{2}[\Delta\phi_1 - p\pi\sin\theta + 2\pi k_1, \Delta\phi_2 - q\pi\sin\theta + 2\pi k_2]\right.$$

$$\left. P^{-1}\begin{bmatrix} \Delta\phi_1 - p\pi\sin\theta + 2\pi k_1 \\ \Delta\phi_2 - q\pi\sin\theta + 2\pi k_2 \end{bmatrix}\right]. \qquad (3.37)$$

Since phase differences are taken as observables, (k_1, k_2) is also an explicit conditioning event as described by the ambiguity diagram. Maximizing $p(\Delta\phi_1, \Delta\phi_2 / \sin\theta, k_1, k_2)$ is equivalent to minimizing the quadratic J.

$$J \triangleq \begin{bmatrix} \Delta\phi_1 - p\pi\sin\theta + 2\pi k_1 \\ \Delta\phi_2 - q\pi\sin\theta + 2\pi k_2 \end{bmatrix}^T P^{-1} \begin{bmatrix} \Delta\phi_1 - p\pi\sin\theta + 2\pi k_1 \\ \Delta\phi_2 - q\pi\sin\theta + 2\pi k_2 \end{bmatrix} \geq 0$$

The minimum of J with respect to the continuous variable $\sin\theta$ and the discrete variables k_1, k_2 can be found by first finding the minimum with respect to $\sin\theta$ for given k_1, k_2, then minimizing the resulting value of J over k_1, k_2, then minimizing the resulting value of J over k_1, k_2. Let $v = \sin\theta$. For given values of k_1, k_2,

$$\left[\frac{\partial J}{\partial v}\right]_{v = \hat{v}} = 0 \text{ gives,}$$

42

$$\hat{v} = \sin\hat{\theta} = \{\pi[p,q]P^{-1}\begin{bmatrix} p \\ q \end{bmatrix}\}^{-1}[p,q]P^{-1}\begin{bmatrix} \Delta\phi_1 + 2\pi k_1 \\ \Delta\phi_2 + 2\pi k_2 \end{bmatrix} \quad (3.38)$$

Applying $\hat{v}$ to J yields

$$J(v = \hat{v}, k_1, k_2)$$

$$= \begin{bmatrix} \Delta\phi_1 + 2\pi k_1 \\ \Delta\phi_2 + 2\pi k_2 \end{bmatrix}^T P^{-1} \begin{bmatrix} \Delta\phi_1 + 2\pi k_1 \\ \Delta\phi_2 + 2\pi k_2 \end{bmatrix}$$

$$- \frac{1}{[p,q]P^{-1}\begin{bmatrix} p \\ q \end{bmatrix}} \{[p,q] P^{-1}\begin{bmatrix} \Delta\phi_1 + 2\pi k_1 \\ \Delta\phi_2 + 2\pi k_2 \end{bmatrix}\}^2$$

$$= f(p,q)\{q\Delta\phi_1 - p\Delta\phi_2 + 2\pi(k_1 q - k_2 p)\}^2$$

$f(p,q)$ does not depend on (k_1, k_2) and is always positive, so to minimize J over (k_1, k_2), we need to minimize the function

$$J' = (q\Delta\phi_1 - p\Delta\phi_2 + 2\pi(k_1 q - k_2 p))^2.$$

Letting $K = k_1 q = k_2 p$, integer K to minimize J' is simply given by,

$$K = -[\frac{1}{2\pi}(q\Delta\phi_1 - p\Delta\phi_2)] \text{ round off} \quad (3.39)$$

Since p,q is a coprime pair, there exist unique values of $k_1.k_2$ such that $K = k_1 q - k_2 p$. Thus, the estimation procedure will be to determine k_1, k_2. Thus, the estimation procedure will be to determine k_1, k_2 as (3.39), and insert these into the expression for $\sin\hat{\theta}$ of (3.38), to find $\hat{\theta}$. Let's examine the performance of this estimator. From the

observation model,

$$q\Delta\phi_1 - p\Delta\phi_2 = q\Delta\phi_{\epsilon 1} - p\Delta\phi_{\epsilon 2} + 2\pi(k_2 p - k_1 q).$$

For any true k_1, k_2, probability that correct K is chosen is given by $|q\Delta\phi_\epsilon^1 - p\Delta\phi_\epsilon^2| < \pi$.

Variance of $(q\Delta\phi_\epsilon^1 - p\Delta\phi_\epsilon^2) = [q, -p]\, P \begin{bmatrix} q \\ -p \end{bmatrix} = [p, -q]\, P \begin{bmatrix} p \\ -q \end{bmatrix}$

$$pr(|q\Delta\phi_\epsilon^1 - p\Delta\phi_\epsilon^2| < \pi) = \text{erf}\left(\frac{\pi}{\left\{[p, -q]\, P \begin{bmatrix} p \\ -q \end{bmatrix}\right\}^{1/2}}\right).$$

Here $\text{erf}(y) = \dfrac{1}{\sqrt{2\pi}} \displaystyle\int_{-y}^{y} e^{-1/2\, x^2}\, dx.$

Thus, probability of gross error

$$= \text{erfc}\left(\frac{\pi}{\left[[p, -q]\, P \begin{bmatrix} p \\ -q \end{bmatrix}\right]^{1/2}}\right) \tag{3.40}$$

In the Mid phase case,

$$p = N, \quad q = M, \quad P = \begin{bmatrix} 2 & -1 \\ -1 & 2 \end{bmatrix} \sigma^2.$$

so that,

$$[p, -q]\, P \begin{bmatrix} p \\ -q \end{bmatrix} = (2M^2 + 2MN + 2N^2)\sigma^2.$$

In the End phase case,

$$p = N, \quad q = M + N, \quad P = \begin{bmatrix} 2 & 1 \\ 1 & 2 \end{bmatrix} \sigma^2$$

so that

44

$$[p, -q] \, P \begin{bmatrix} p \\ -q \end{bmatrix} = (2M^2 + 2MN + 2N^2)\sigma^2.$$

Therefore the probability of gross error depends only on the sensor separations, and not on whether Mid or End phase configuration is used. In either case, probability of gross error is,

$$Pr = erfc\left[\frac{\pi}{\sqrt{2}\sigma(M^2 + MN + N^2)^{1/2}}\right] \tag{3.41}$$

The mean square error in fine resolution is given by Cramer-Rao lower bound;

$$\sigma^2_{\sin\theta} = \left[E\left\{\frac{\partial^2}{\partial(\sin\theta)^2} \ln(p(\Delta\phi_1, \Delta\phi_2/\sin\theta, k_1 k_2))\right\}\right]^{-1}$$

$$= \frac{1}{\pi^2}\left[[p,q]P^{-1}\begin{bmatrix} p \\ q \end{bmatrix}\right]^{-1}$$

which, like probability of gross error, is identical for Mid and End phase processing,

$$\sigma^2_{\sin\theta} = \frac{3\sigma^2}{2\pi(M^2 + MN + N^2)} \tag{3.42}$$

Since $erfc(\cdot)$ is a monotonically decreasing function of argument, increasing $(M^2 + MN + N^2)$ will increase probability of gross error, while decreasing $\sigma^2_{\sin\theta}$. From this, it is apparent that any choice of sensor spacings represents a trade off between minimizing probability of gross error and maximizing fine resolution accuracy.

3.4. Case IV [10]

The maximum likelihood estimate can also be used for

multiple source location [11]. But we will refer to a
different approach for the purpose of this survey. In
this referenced paper, the problem of simultaneous angular
location of multiple sources with a linear antenna array
is formulated as follows.
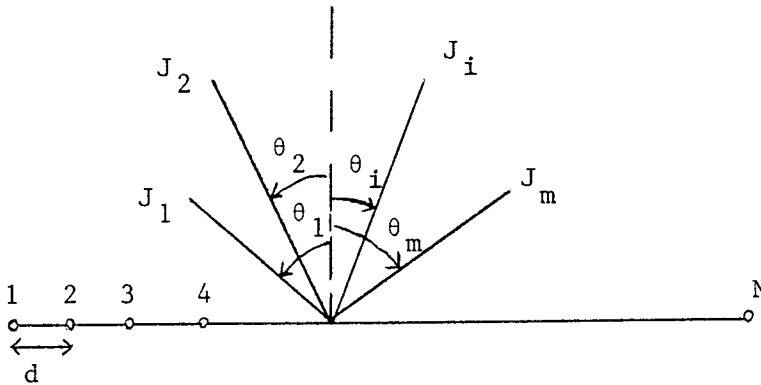
Fig. 3.8. Linear array and signal sources.

N isotropic sensors are unfirmly distributed with spacing
d. The array is operated in a narrowband mode at center
frequency whose wavelength is λ. There are m signal
sources $J_1, J_2, \ldots, J_m$ located with angles $\theta_1, \theta_2, \ldots, \theta_m$ with
the antenna normal. Provisions have been made to measure
quadratures at the output of each sensor. Observed
complex envelope $\vec{z}$ is given, from the configuration, as:

$$
\begin{bmatrix} z_1 \\ z_2 \\ \cdot \\ \cdot \\ \cdot \\ \cdot \\ \cdot \\ z_N \end{bmatrix} = \begin{bmatrix} v_1 & v_2 & & v_m \end{bmatrix} \begin{bmatrix} S_1 \\ S_2 \\ \cdot \\ \cdot \\ \cdot \\ \cdot \\ \cdot \\ S_m \end{bmatrix} + \begin{bmatrix} g_1 \\ g_2 \\ \cdot \\ \cdot \\ \cdot \\ \cdot \\ g_N \end{bmatrix} \qquad (3.43)
$$

$$
\text{where} \quad v_i = \begin{bmatrix} 1 \\ \exp(j\frac{2\pi}{\lambda}d\ \sin\ \theta_1) \\ \exp(j\frac{4\pi}{\lambda}d\ \sin\ \theta_i) \\ \cdot \\ \cdot \\ \cdot \\ \exp(j(N-1)\frac{2\pi}{\lambda}d\ \sin\ \theta_i) \end{bmatrix} = \begin{bmatrix} 1 \\ t \\ t^2 \\ \\ \\ t^{N-1} \end{bmatrix}
$$

z_i: resultant complex envelope observed at the output of ith sensor ($i = 1,2,\ldots,N$).

S_j: complex envelope from j^{th} signal source at the reference sensor ($j = 1,2,\ldots,m$).

g_i: complex envelope of receiver noise at the ith sensor ($i = 1,2,\ldots,N$).

Statistical assumptions are such that,

$E(g_i) = 0$, $E(g_i^* g_j) = \delta_{i,j}\ g^2$, $E(g_i^* S_j) = 0$, $E(S_i) = 0$.

Let $[v_1,v_2,\ldots,v_m] = [V]$. Covariance matrix C of joint observations $\vec{z}$ is,

$$
C \triangleq E(\vec{z}\ \vec{z}^+) = g^2 I + V \cdot E(\vec{S} \cdot \vec{S}^T) \cdot V^+ \qquad (3.44)
$$

Given sampled covariance C, the problem is to evaluate

the number of signal sources and their angular locations

using (3.44). A theoretical basis is presented in this

paper, using the properties of Vandermonde vectors.

Basically the algorithm consists of determining the eigen-

values, eigenvectors of complex covariance matrix obtained

from the sampled output signals of linear array and

solving a polynomial equation whose coefficients are

obtained from the eigenvectors. The vector of the form,

$(1, t, t^2, \ldots, t^{k-1})^T$ is referred to as a Vandermonde vector

and is denoted by $v_k(t)$.

Lemma 1. Vectors $v_k(t_i)$, $i = 1, 2, \ldots, \ell$ are linearly

independent for $k \geq \ell$, where $t_i \neq t_j$ for $i \neq j$.

Proof. Consider the matrix below.

$$
\begin{bmatrix}
1 & 1 & 1 \\
t_1 & t_2 & t \\
t_1^2 & t_2^2 & t_\ell^2 \\
\cdot & & \\
\cdot & & \\
\cdot & & \\
t_1^{k-1} & t_2^{k-1} & t_\ell^{k-1}
\end{bmatrix}
$$

Since the column rank of a matrix is the same as its row

rank, consider the square matrix formed by extracting the

first ℓ rows. The determinant of this Vandermonde matrix

does not vanish when $t_i \neq t_j$ for $i \neq j$.

Theorem 1. Let $\{\vec{x}_1, \vec{x}_2, \ldots, \vec{x}_\ell\}$ be a set of linearly

independent k-tuples with Vandermonde basis
$\{v_k(\alpha_1), v_k(\alpha_2), \ldots v_k(\alpha_\ell)\}$, $k > \ell$. Let $F = [\vec{x}_1, \vec{x}_2, \ldots, \vec{x}_\ell]$

$$
= \begin{bmatrix} w_1^T \\ w_2^T \\ \cdot \\ \cdot \\ \cdot \\ \cdot \\ w_k^T \end{bmatrix} = \begin{bmatrix} W \\ --- \\ w_k^T \end{bmatrix} .
$$

Assume W has a rank ℓ. Construct polynomials $G(x) = w_k^T (W^+W)^{-1} W^+ v_{k-1}(x) - x^{k-1}$ and $g_i(x) = w_i^T (W^+W)^{-1} W^+ v_{k-1}(x) - x^{i-1}$ for $i = 1, 2, \ldots, k-1$. Then

$f(x) = \gcd(G(x), g_1(x), \ldots, g_{k-1}(x))$ possesses $\alpha_1, \alpha_2, \ldots \alpha_\ell$ as its only roots (where gcd means greatest common divisor).

<u>Proof</u>. The existence of Vandermonde basis implies the existence of set, $(\alpha, y_1, y_2, \ldots y_\ell)$ satisfying the following k nonlinear equations

$$v_k(\alpha) = F y \qquad (3.45)$$

where $y = (y_1, y_2, \ldots, y_\ell)^T$. Rewrite (3.45) as

$$W y = v_{k-1}(\alpha)$$

$$ \qquad (3.46)$$

$$w_k^T y = \alpha^{k-1}$$

Since a consistent solution y exists, y can be written as $y = (W^+W)^{-1} W^+ v_{k-1}(\alpha)$, and let $G(\alpha)$ be such that $G(\alpha) =$

49

$$w_k^T(W^+W)^{-1}W^+v_{k-1}(\alpha) - \alpha^{k-1}$$

$G(\alpha)$ possesses $\alpha_1, \alpha_2, \ldots, \alpha_\ell$ and $(k-\ell-1)$ extraneous roots. Desired root also satisfy $Wy = v_{k-1}(\alpha)$. Hence,

$$W(W^+W)^{-1}W^+v_{k-1}(\alpha) = v_{k-1}(\alpha), \quad [W(W^+W)^{-1}W^+ - I]v_{k-1}(\alpha) = 0$$

from which one can obtain polynomials $g_i(\alpha)$, $i = 1, 2, \ldots,$ $k-1$. Thus $f(x) = \gcd\{G(x), g_i(x); i = 1, 2, \ldots, k-1\}$ should include as its roots $\alpha_1, \alpha_2, \ldots, \alpha_\ell$. If α' is a root of $f(x)$, y can be found such that $Fy = v_k(\alpha')$. If $\alpha' \notin (\alpha_1, \alpha_2, \ldots, \alpha_\ell)$, then there exist more than ℓ linearly independent Vandermonde vectors, from Lemma 1 (since $k > \ell$). A contradiction. Thus the only roots of $f(x)$ are

$\alpha_1, \alpha_2, \ldots, \alpha_\ell$.

<u>Corollary 1.</u> If vectors $\vec{x}_1, \vec{x}_2, \ldots, \vec{x}_\ell$ are orthonormal, then $G(x) = w_k^T W^+ v_{k-1}(x) - (1-\lambda)x^{k-1}$, and $g_i(x) = w_i^T(I + (1-\lambda)^{-1}w_k^* w_k^T)W^+ v_{k-1}(x) - x^{i-1}$ where $\lambda = |w_k|^2$.

<u>Proof.</u> Since $\vec{x}_i$'s are orthonormal, $F^+F = W^+W + w_k^* w_k^T = I$. $(W^+W)^{-1} = (I - w_k^* w_k^T)^{-1} = I + (1-\lambda)^{-1}w_k^* w_k^T$.

Inserting $(W^+W)^{-1}$ into expressions in Theorem 1 yields the result.

In the case where W does not have rank ℓ, the following modification has to be performed. Since F has a column rank ℓ, and row rank ℓ, a w_p^T can always be found such that W_p has a rank ℓ, that is,

$$F_p = \begin{bmatrix} W_p \\ w_p^T \end{bmatrix}$$

where F_p is obtained by deleting w_p^T from its original

50

position, and putting w_p^T next to the last row, and W_p has rank ℓ. Define

$$v_{k-1}^p(x) = (1, x, x^2, \ldots, x^{p-2}, x^p, \ldots, x^{k-1}).$$

<u>Theorem 2</u>. Construct polynomials $G(x) = w_p^T(W_p^+ W_p)^{-1}$ $\cdot W_p^+ v_p^{k-1}(x) - x^{p-1}$ and $g_i(x) = w_i^T(W_p^+ W_p)^{-1} W_p^+ v_{k-1}^p(x) - x^{i-1}$, for $i = 1, 2, \ldots, k$, $i \neq p$. Then $f(x) = \gcd \{G(x), g_i(x)\}$ possesses $\alpha_1, \alpha_2, \ldots, \alpha_\ell$ as its only roots.

<u>Proof</u>. Since the rows of F have been permuted, the elements of $v_k(\alpha)$ has to be permuted accordingly.

<u>Corollary 2</u>. For $k = \ell + 1$, $g_i(x) = 0$ and hence $f(x) = G(x)$, and degree of $f(x)$ is ℓ.

<u>Proof</u>. $\vec{g}(\alpha) = [W(W^+W)^{-1} W^+ - I] v_{k-1}(\alpha)$, where W is nonsingular matrix. Thus $\vec{g}(\alpha) = \vec{0}$.

Based on the theory described so far, let's consider the problem of multiple source location. Consider covariance matrix C of (3.44).

$$C = g^2 I + V \cdot E(\vec{S} \ \vec{S}^+) V^+$$

$$= g^2 I + V \cdot A \cdot V^+ = g^2 I + B.$$

We assume that source signal covariance matrix A is positive definite, also number of sensors N is greater than the number of sources m. To show that eigenvectors of received signal covariance matrix B can be expressed as linear combinations of v_i's, assume $\vec{e} = V \cdot \vec{p}$ is eigenvector of B and hence C. Then we should have $B \cdot \vec{e} = \lambda \vec{e}$, i.e.,

51

$$VAV^+V\vec{p} = \lambda V \cdot \vec{p}; \quad \text{Let } V^+V = \Lambda$$

$$VA\Lambda\vec{p} = \lambda \cdot V \cdot \vec{p}$$

$$V(A\Lambda - \lambda I)\vec{p} = \vec{0} \quad (A\Lambda - \lambda I)\vec{p} = \vec{0}.$$

Since $\vec{v}_i$'s are set of m linearly independent vectors. Thus nontrivial eigenvalues of B are the same as those of $A\Lambda$. Since both Λ and A have rank m, it follows that B has m nonzero eigenvalues. Also, these eigenvalues are positive since A, Λ are both positive definite. Since $C = g^2 I + B$, C has m eigenvalues greater than g^2.

Thus, the problem of multiple source location is solved by first obtaining eigenvalues of sampled covariance matrix C, and eigenvectors associated with eigenvalues($>g^2$). Then apply Theorem 1 or Corollary 1 to obtain v_i's. In this case, since the roots is of the form $\exp\{j2\pi d/\lambda \sin\theta\}$, we can restrict our search for the roots to points on the unit circle.

Consider the situation where noise assumption $g^2 \cdot I$ is not true. In this case, the desired roots of G(x) and $g_i(x)$ do not exactly lie on the unit circle and we seek to find the least square error solution satisfying the system of nonlinear equations. Let the system of nonlinear equations be $Gv_k(x) = 0$. We minimize $\Phi = v_k^+(x)G^+Gv_k(x)$ subject to the constraint that $x = e^{j\theta}$.

In this reference paper, Reddi also considered the case when the source covariance matrix A is singular, due to multipath phenomenon and various other reasons.

52

In closing this chapter, it should be mentioned that there is a vast amount of algorithms in the field of array signal processings,

4. SEQUENTIAL LIKELIHOOD ALGORITHM FOR INTERFEROMETER

In this chapter, we will develope a sequential likelihood algorithm for a linear horizontal interferometer.

4.1 Array and receiver model

The coordinate system of the array is described by Fig. 4.1 below.
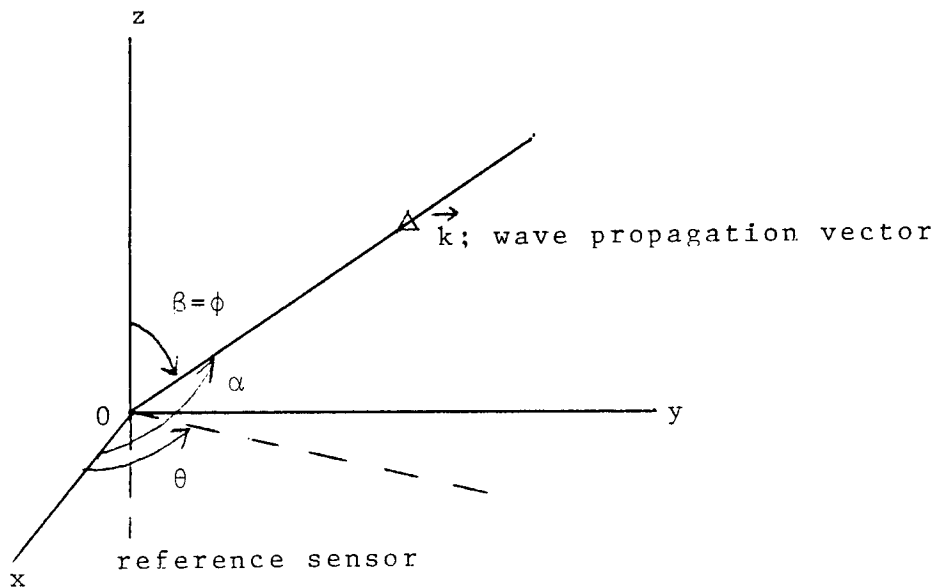
Fig. 4.1. Horizontal interferometer and coordinates.

The direction cosines, μ_1 and μ_2, are defined as in Fig. 2.2, and given by

$$\begin{bmatrix} \mu_1 \\ \mu_2 \end{bmatrix} = \begin{bmatrix} \cos\ \alpha \\ \cos\ \beta \end{bmatrix} = \begin{bmatrix} \sin\phi \cdot \cos\theta \\ \cos\phi \end{bmatrix} \quad ,$$

where μ_2 is assumed to be slowly changing.

In the above array, the ith sensor is located at the position $(d_i,0,0)$, and its output voltage as a function of time is

54

given by $r_i(t)$.

Fig. 4.2 represents our prototype configuration of the associated i^{th} channel, when the waveform received is pulse-modulated with pulse width T. Although the automatic gain control can be incorporated so as to maintain a constant video level of the IF signal at p_o, the effect of AGC will not be considered in this work. The Doppler shift, due to a motion of the emitter, is assumed to be compensated by the common reference signal of Fig. 4.2 (i.e., $f = f_o + f_d$) or through a demodulation in general. Also the effect of spectrum spread (, due to a short duration of pulse) on the effective receiver noise is assumed negligible. The observation rate is assumed to be at the typical order of 1 KHZ. In establishing the sequential algorithm, the quadratures at p_3 are used as observations because the sequential algorithm replaces the role of low pass filter.
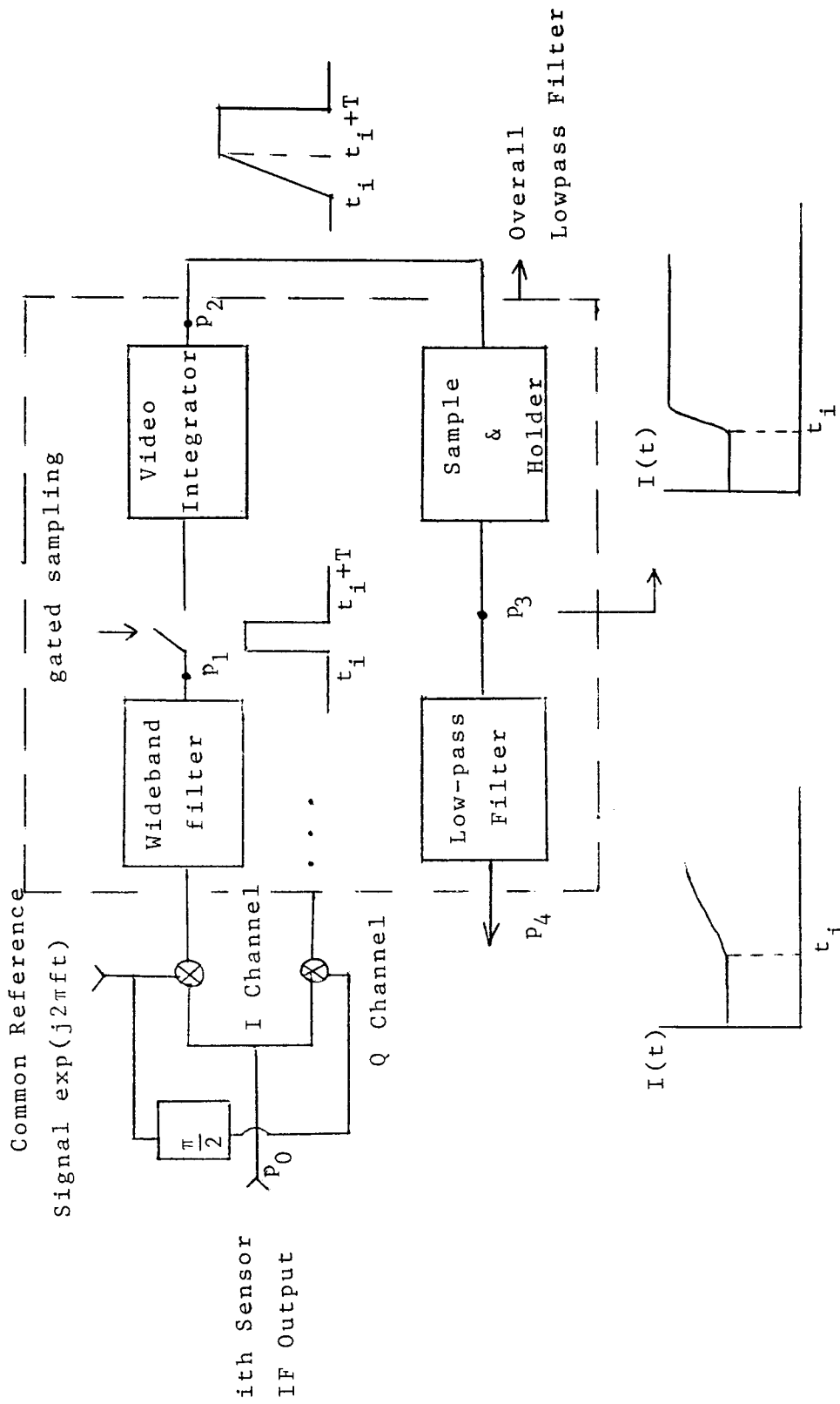
Fig. 4.2. Configurations of RCVR at the ith channel.

4.2 Observed signal model

With the receiver structure in mind, the IF output of the ith sensor $r^i(t)$ can be represented in terms of the complex envelope,

$$r^i(t) = Re(\tilde{r}^i(t)exp(j\ 2\pi ft)), \qquad (4.1)$$

where $\tilde{r}^i(t)$ is the complex envelope of $r^i(t)$, and is expressed with the common reference signal providing the phase reference.

In the description of the observed signal model, we do not consider the variations of antenna gains for different directions of arrivals, and also the differential delays due to different paths of propagation are assumed negligible.

The first portion of the received signal, the directly incident portion, is given by,

$$\tilde{S}_F^i(t) = A^d(t)exp(j\varphi^d(t))\cdot p(t)\cdot(exp(jk_o\mu_1\cdot d_i), \qquad (4.2)$$

where $k_o = \dfrac{2\pi}{\lambda}$.

If processing at the level of random variables is desired, one can treat $A^d exp(j\varphi^d)$ as a complex random variable, whose quadratures are independently gaussian with identical probability densities. Later, sample values of $A^d exp(j\varphi^d)$ are to be properly defined through the integration over the pulse-width (see (4.13)). According to this model, the amplitude is Rayleigh distributed and phase is uniformly distributed on $(0,\ 2\pi)$. Although the amplitude is not always fluctuating, the distribution of phase is uniform due to fluctuating factors such as slight variation of

57

emitter position or fluctuating phase of source signal at each transmitting sequence.

For the sequential algorithm developed in this work, let's assume that $A^d(t)$ is a slowly varying function of time. We say "function of time" in terms of discrete basis in time, which will be clear in (4.13), (4.16). In (4.2), $p(t)$ represents a pulse modulation;

$$p(t) = \begin{cases} 1 & \text{for } t\varepsilon(t_i, t_i + T) \\ 0 & \text{otherwise,} \end{cases}$$

where t_i's are arrival times of the signal of interest.

The second portion of the received signal is the specular multipath return and is given by

$$\tilde{s}_s^i(t) = A^d(t) \cdot \exp(j\varphi^d(t)) \cdot p(t) \cdot \exp(jk_o\mu_1 \cdot d_i) \cdot \rho_s^i(\phi) \cdot \exp(j\varphi_s^i(t)) \tag{4.3}$$

where,

ρ_s^i: amplitude of the overall terrain reflection coefficient, which is a function of elevation and effective roughness.

$\rho_s^i = \rho_s$ for all i.

φ_s^i: $\varphi_s^i = \gamma^i + k_o \cdot 2h_i \cos \phi$ for most of the geometries, where the specular returns are important.

γ_i: phase shift due to the complext reflection coefficient of ground. $\gamma^i = \gamma$ for all i.

58

$k_o \cdot 2h_i \sin \phi$: phase shift, due to the path length

difference between the direct ray and

the specular one. $h_i = h$ for all i.

φ_s^i equals φ_s for all i in horizontal interferometer. In reality, the observed specular component at each sensor will fluctuate along sensors of the array, because each geometrical center of first Fresnel regions, associated with each sensor, is slightly separated with each other on the rough surface. As explained in Chapter 2, it should be reasonable to assume a strong phase coherences between the specular components, considering the modelling of the specular components.

In a linear horizontal array, it is convenient to combine the direct portion with the specular return. Thus,

$$\tilde{s}^i(t) = A^d(t) \cdot \exp(j\varphi^d(t) \cdot (1 + \rho_s \exp(j\varphi_s(t))) \cdot p(t) \cdot \exp(jk_o \mu_1 \cdot d_i)$$

$$= A(t) \cdot \exp(j\varphi(t)) \cdot p(t) \cdot \exp(jk_o \mu_1 \cdot d_i) \qquad (4.4)$$

We will treat $\tilde{s}^i(t)$ either as an unknown deterministic function of time or as a complex gaussian process whose quadratures are i.i.d. gaussian with mean zero, and locally wide-sense stationary with low pass spectra. However, even when $\tilde{s}^i(t)$ can be approximately gaussian process under a given situation, the actual choice of model for $\tilde{s}^i(t)$ depends on the length of the processing period as is compared to correlation time of given $\tilde{s}^i(t)$.

As a remark, when there exist several of the specular returns from a given terrain, these can be parts of $\tilde{s}^i(t)$. Specifically, each specular return with direction cosine

$\vec{\mu}_i$ can be characterized by a planewave along the sensors of the array, and is independent of the other specular return with a different direction cosine $\vec{\mu}_j$ in their phase relationship. Further, if the resultant $\tilde{s}^i(t)$ is regarded as a complex gaussian process at each sensor, joint observation set of the array is described by spatial covariance matrix which depends on the direction cosines, $\vec{\mu}_i$'s. This case is an example of a spatially dispersive channel, the adversary effect of which may well be severe [17]. Since $\vec{\mu}_i$ irregularly depends on $\vec{\mu}$(the source direction) in nonhomogeneous surface, a priori knowledge of the spatial covariance matrix is required to set up the maximum likelihood estimator. If a local range of $\vec{\mu}$ is of interest, we may use same measured spatial covariance for that interval of $\vec{\mu}$.

The diffuse component can also be characterized using the same format. However, the diffuse component is assumed to come from a continuum of directions and not just one like the free space and specular returns. To represent this continuum, we use an integral representation in the following form.

$$\tilde{s}^i_d(t) = A^d(t)\int_{-1}^{1}[\int_{-1}^{1} p\vec{\mu}'(t)\ M^i(\vec{\mu},\vec{\mu}',t)\exp(jk_o\mu_1'\cdot d_i)d\mu_2']d\mu_1' \qquad (4.5.1)$$

$$= A^d(t)\cdot\sigma^i_d(t)\cdot\tilde{b}^i(t)\cdot\exp(jk_o\mu_1\cdot d_i) \qquad (4.5.2)$$

$$= m^i_1(t) + j\ m^i_2(t)$$

where $A^d(t)$ in (4.5) is an expression for convenience, considering the varying factors separately involved in the multipath-induced paths.

In (4.5),

$p_{\vec{\mu}'}(t)$: spread in the arrival time of elemental

diffuse component coming from the direction

$\vec{\mu}'$

$M^i(\vec{\mu},\vec{\mu}',t)$: complex envelope of the elemental diffuse

component expressed relative to

$\exp(j(k_o \cdot \mu'_1 \cdot d_i + 2\pi ft))$. Quadrature

components are i.i.d., zero mean, gaussian,

and locally wide-sense stationary with

following covariance assumption.

$$E(M^i(\vec{\mu},\vec{\mu}',t')M^j(\vec{\mu},\vec{\mu}'',t'')^*) = f_{i,j}(\vec{\mu},\vec{\mu}',t' - t'')\delta(\vec{\mu}' - \vec{\mu}'')$$

$$(4.6)$$

$$f_{i,i}(\vec{\mu},\vec{\mu}',0) \triangleq K(\vec{\mu},\vec{\mu}') \quad \text{for all i.} \qquad (4.7)$$

This covariance states that radiation fields coming from

different directions are independent. Spatial independence

corresponds to $f_{i,j} = f \cdot \delta_{i,j}$. $K(\vec{\mu},\vec{\mu}')$ is the so called

channel spread function [12], and is normalized with respect

to intensity of direct signal.

The CSF represents direction spread of the given

observed signal, due to the diffuse component. The model

(4.5) is different from T.P. Mcgarty's model in that we

allow $M^i(\vec{\mu},\vec{\mu}',t)$'s to be a set of the spatially correlated

random variables at each t, rather than treating $M^i(\vec{\mu},\vec{\mu}',t) = $

$M(\vec{\mu},\vec{\mu}',t)$ for all i which is not the proper expression for

the diffuse component [12].

Expressing (4.5.1) in terms of spherical coordinates

(θ,ϕ),

$$\tilde{s}_d^i(t) = A^d(t) \int_{-\pi}^{\pi}\int_0^{\pi} p_{\theta',\phi'}(t) M^i(\theta,\phi;\theta',\phi') \exp(jk_o \cdot \mu_1' \cdot d_i) d\phi' d\theta' \tag{4.8}$$

$$E|M^i(\theta.\phi;\theta',\phi')|^2 = K(\theta,\phi,\theta',\phi') \tag{4.9}$$

$$\int_0^{\pi} K(\theta,\phi;\theta',\phi') d\phi' = K_1(\theta,\phi;\theta'). \tag{4.10}$$

Assuming isotropic and homogeneous rough surface, $K(\theta,\phi;\theta')$ takes maximum at $\theta = \theta'$ source azimuth, and is a function of $|\theta - \theta'|$ for given ϕ. A detailed explanation of the CSF, relation between $K(\vec{\mu},\vec{\mu}')$ and $K(\theta,\phi)$, and the assumed properties of the spatial correlation are given in the next sections. In (4.6), the time dependence of $f_{i,j}(\vec{\mu},\vec{\mu}', t' - t'')$ comes from fluctuating factors such as relative motion of the emitter or fluctuation of rough surface (e.g., ocean surface, vegetation motion). The expression (4.5.2) is a simpler description of the diffuse component from a homogeneous rough surface.

σ_d^i: standard deviation of quadratures of the diffuse component at the ith sensor, normalized with respect to intensity of direct component, and also independent of μ_1, given μ_2.

$$\sigma_d^i = \sigma_d^o \cdot R(\phi) = \sigma_d \text{ for all } i \tag{4.11}$$

σ_d^o: function of the apparent roughness $\dfrac{\sigma\cos\phi}{\lambda}$.

$R(\phi)$: Fresnel reflection coefficient for smooth earth with absorption loss considered.

$\tilde{b}^i(t)$: normalized complex gaussian process, spatially correlated in general.

The final term in the observed signal is the RCVR noise
component $\tilde{w}^i(t)$. Thus the observed signal at the ith sensor
is,

$$\tilde{r}^i(t) = \tilde{S}^i(t) + \tilde{S}_D^i(t) + \tilde{w}^i(t). \tag{4.12}$$

It is convenient to deal with an integrated form of
$\tilde{r}^i(t)$. Integration of $\tilde{r}^i(t)$ is depicted in Figure 4.1 and
is equivalent to a demodulation in general.

$$\tilde{r}^i(t_i) \triangleq \frac{1}{T} \int_{t_i}^{t_i+T} \tilde{r}^i(t)\,dt \tag{4.13}$$

where t_i is written in an approximate sense. Thus, the
integrated diffuse component is,

$$\tilde{S}_D^i(t_i) = A^d(t_i) \iint g(\vec{\mu}')\cdot M^i(\vec{\mu},\vec{\mu}',t_i)\cdot\exp(jk_o\mu_1'd_i)\,d\mu_1'\,d\mu_2' \tag{4.14}$$

where $M^i(\vec{\mu},\vec{\mu}',t) \simeq M^i(\vec{\mu},\vec{\mu}',t_i)$, due to its low-pass character
as compared to a typical pulse width T.

$$g(\vec{\mu}') = \frac{1}{T} \int_{t_i}^{t_i+T} p_{\vec{\mu}'}(t)\,dt \tag{4.15}$$

$g(\vec{\mu}')$ is almost 1 over most viewing directions $\vec{\mu}'$. Thus
the term "$p_{\vec{\mu}'}(t)$", due to differential delay, is eliminated.
In summary, letting $\vec{m}(\mu_1)$ be $\begin{bmatrix} 1 \\ \exp(jk_o\mu_1\cdot d_1) \\ \vdots \\ \exp(jk_o\mu_1\cdot d_N) \end{bmatrix}$, we obtain

$$\vec{r}(t_i) = A(t_i)\exp(j\varphi(t_i))\vec{m}(\mu_1) + A^d(t_i)\iint M(\vec{\mu},\vec{\mu}',t_i)\vec{m}(\mu_1')\cdot$$

$$\cdot d\mu_1'\,d\mu_2' + \vec{w}(t_i) \tag{4.16}$$

where,

$$\vec{w}(t_i) \triangleq \frac{1}{T} \int_{t_i}^{t_i+T} \vec{w}(t)dt \qquad (4.17)$$

$$E(\vec{w}(t_i)\vec{w}^+(t_j)) = N_o \cdot I \cdot R(t_i - t_j)$$

$M(\vec{\mu},\vec{\mu},t_i) =$ Diagonal Matrix with $M^i(\vec{\mu},\vec{\mu}',t_i)$ being

a diagonal element.

The joint observation set $\vec{r}(t_i)$ is the output of sample and holder at p_3 of Fig. 4.2.

Considering a sampling rate, typically at the order of 1 KHZ, $\vec{w}(t_i)$ is virtually discrete white gaussian process with $R(t_i - t_j) = \delta(t_i - t_j)$ in (4.17).

4.3. The channel spread function

From the definition of channel spread function $K(\vec{\mu},\vec{\mu}')$ (Eq. (4.7)) and $K(\vec{\theta},\vec{\theta}')$ (Eq. (4.9)),

$$\iint K(\vec{\mu},\vec{\mu}')d\mu_1' d\mu_2' = \iint K(\vec{\theta},\vec{\theta}')d\theta' d\phi'.$$

Thus $K(\vec{\mu},\vec{\mu}') = K(\vec{\theta},\vec{\theta}') \left| \dfrac{d\theta d\phi}{d\mu_1 d\mu_2} \right|_{\theta',\phi'}$, $\qquad (4.18)$

where $J = \left| \dfrac{d\theta d\phi}{d\mu_1 d\mu_2} \right|$ is a Jacobian. Thus, once $K(\vec{\theta},\vec{\theta}')$ is obtained, the CSF $K(\vec{\mu},\vec{\mu}')$ follows directly from Eq. (4.18).

We will refer to T.P. Mcgarty's work [12] in the description of $K(\vec{\theta},\vec{\theta}')$, which is more rigorous than the similar expression in Chapter 2 (i.e., elevation power density).

For a notational convenience, we will use (θ,ϕ) for (θ',ϕ') with emitter located at $(\frac{\pi}{2},\phi_o)$ in this section. Consider radiation coming to the sensor R from solid angle

$\phi, \phi + d\phi$ and $\theta + d\theta$ in Fig. 4.3. If we let $\phi = \tilde{\phi} + \frac{\pi}{2}(\tilde{\phi} > 0)$, then this solid angle generates a surface area dA from which power must be scattered so as to be received from this direction. Let $\vec{r}_1$ be a vector from the emitter at T to the center of dA, and $\vec{r}_2$ a vector from the center of dA to the sensor R. Radiation patterns of antennas are assumed to be isotropic.
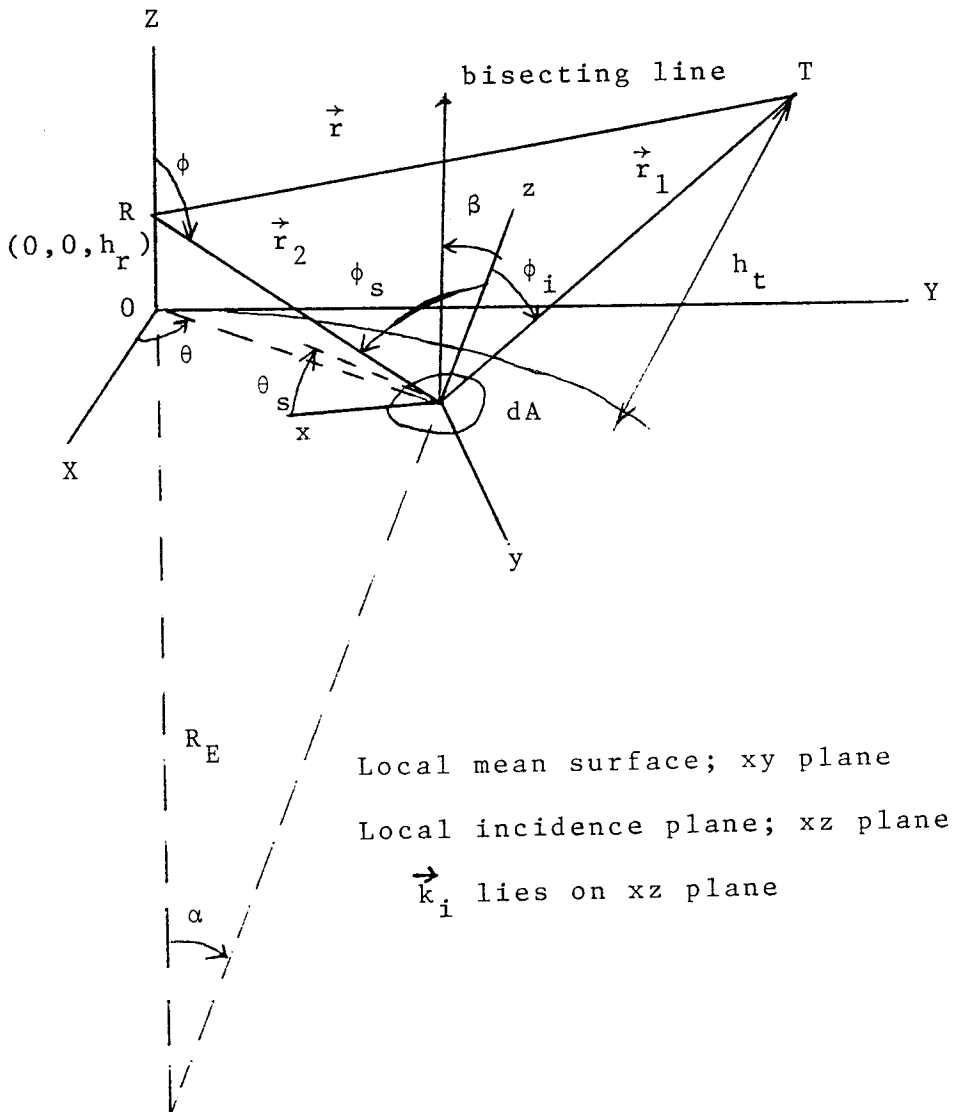
Local mean surface; xy plane

Local incidence plane; xz plane

$\vec{k}_i$ lies on xz plane

Fig. 4.3. Spherical earth-scattering geometry.

65

Let $\vec{k}_i$ represent the wave vector defining the direction of radiation coming from T to dA, and $\vec{k}_s$ the wave vector defining propagation from dA to R. Define a scattering cross section per unit area as $\sigma_b(\vec{k}_s, \vec{k}_i)$. The power at R is $\dfrac{p_o}{(4\pi)^2 r_1^2 r_2^2} \sigma_b(\vec{k}_i, \vec{k}_s) dA$; p_o is transmitter power. From the definition of $K(\theta, \phi)$,

$$K(\theta, \phi) = \frac{p_o \cdot \sigma_b(\vec{k}_i, \vec{k}_s)}{(4\pi)^2 r_1^2 r_2^2} \cdot \left| \frac{dA}{d\theta d\phi} \right| \bigg/ \frac{p_o}{4\pi r^2}$$

$$= \frac{1}{(4\pi)} \left(\frac{r}{r_1 r_2} \right)^2 \cdot \sigma_b(\vec{k}_i, \vec{k}_s) \cdot \left| dA/d\theta d\phi \right|. \qquad (4.19)$$

where θ and ϕ are azimuth and elevation with respect to R. $\sigma_b(\vec{k}_i, \vec{k}_s)$ depends on the nature of the scattering surface and $\left| dA/d\theta d\phi \right|$ is a Jacobian. Each of these terms will now be evaluated starting with the scattering cross section.

Let $\xi(x, y)$ be the height of the surface, which is normally distributed with Eqs. (2.4), (2.5). The correlation function of the surface has been chosen to satisfy certain regularity conditions for Kirchhoff approximation. Barrick [13] has obtained an expression for the scattering cross section per unit area. It is given as

$$\sigma_b(\vec{k}_i, \vec{k}_s) = \pi n_A \cdot p \cdot \left| R(\vec{k}_i, \vec{k}_s) \right|^2 \qquad (4.20)$$

where n_A is the average number of specular reflectors per unit area. p is the average absolute value of the product of the principal radii of curvature at specular points and $\left| R(\vec{k}_i, \vec{k}_s) \right|^2$ is the reflection coefficient giving the depolarization loss from a tilted surface. Following

Barrick's result,

$$n_A = (7.255/\pi^2 T^2) \exp(-\tan^2 \beta / \tan^2 \beta_o).$$

$$\tan \beta = (\sin^2 \phi_i - 2 \sin \phi_i \sin \phi_s \cos \theta_s + \sin^2 \phi_s)^{1/2} /$$

$$(\cos \phi_i + \cos \phi_s)$$

where β is the angle between the local normal on dA and
the local surface normal at the specular point.

Note that n_A represents a density of specular scatterers
per unit area, and it depends on the location of surface
through β and the statistical characteristics of the
surface. For surfaces with large slope $\tan \beta_o$, n_A can tend
to be large. Also p is given by $p = 0.1378 (T^2/\tan^2 \beta_o) \sec^4 \beta$.

As a result, $\sigma_b(\vec{k}_i, \vec{k}_s)$ depends on $\tan \beta_o (\frac{2}{T} \sigma)$ as a
parameter, is independent of σ and T separately as in
Chapter 2, and it is independent of wavelength, due to
the specular (optical) point approximation.

The reflection coefficient has been evaluated by
Mitzner [14].

For horizontal-to-horizontal or vertical-to-vertical
polarization, we have (with omitting Fresnel reflection
coefficient),

$$R^2(\vec{k}_i, \vec{k}_s) = (-\sin \phi_i \sin \phi_s \sin^2 \theta_s + a_2 a_3)/4 \sin^2 \xi \cos^2 \xi$$

with

$$\cos \xi = (1 - \sin \phi_i \sin \phi_s \cos \theta_s + \cos \phi_i \cos \phi_s)^{1/2}/2$$

$$a_2 = \cos \phi_i \sin \phi_s + \sin \phi_i \cos \phi_s \cos \theta_s$$

67

$$a_3 = \sin\phi_i \cos\phi_s + \cos\phi_i \sin\phi_s \cos\theta_s.$$

But additionally, $R^2(\vec{k}_i, \vec{k}_s)$ has to be modified by considering the actual inclination of the antenna axis in this case. The model (4.20) is valid under the following constraints.

(1) The radius of the surface curvature is large compared to a wavelength. Hence the tangent plane approximation can be applied.

(2) Multiple scattering can be neglected. The problems associated with multiple scattering are significant in low angle geometry.

(3) $(k\sigma \cos\phi_i)^2 \gg 1$; the surface is apparently very rough. This allows us to sum the power from each specular point incoherently.

$|dA/d\theta d\phi|$ in Eq. (4.19) relates the incremental surface area to the solid angle that generates it, and is given by

$$\left|\frac{dA}{d\theta d\phi}\right| = r_2^2 / \{\csc^2\alpha - \csc\alpha \cot[(h_r/R_E) + 1]\}/\sin\alpha.$$

Thus the spatial spectrum of the field is

$$K(\theta,\phi) = \frac{1}{4\pi}\left(\frac{r}{r_1}\right)^2 \sigma(\theta_s, \phi_s, \phi_i)\left|\frac{\sin\alpha}{1 - \cos\alpha(1 + \frac{h_r}{R_E})}\right|$$

where θ_s, ϕ_s, ϕ_i, and α all are defined in terms of θ and ϕ, given the position of emitter.

When the surface is rough, the very nature of the roughness acts as a shadowing mechanism that prevents the incident radiation from falling on a reflecting surface. Furthermore, when the radiation is scattered, it may also find itself shadowed from the receiving point, a result of

the same phenomenon. Wagner [15] has derived the function $S(\phi_i, \phi_s)$ which is the probability that a ray incident from angle ϕ_i does not get blocked and generate a scattered ray in direction ϕ_s, which is also not blocked. This function, called the shadowing function, is given by

$$S(\phi_i, \phi_s) = \{1 - \exp[-2(B_i + B_s)]\} \cdot [\text{erf}(\nu_i) + \text{erf}(\nu_s)] / [4(B_i + B_s)],$$

where

$$B_k = [\exp(-\nu_k^2) - \sqrt{\pi}\, \nu_k \, \text{erfc}(\nu_k)] / \sqrt{\pi}\nu_k$$

$$\nu_k = |\cot\phi_k| / \sqrt{2 \cdot \tan^2\beta_o}$$

$k = i$ or s, and erf is the standard error function. This function gives the portion of the total number of specular points both not shadowed and not blocked. However, closer to grazing, other corrections besides shadowing must also be included because constraints (2), (3) generally fail.

In Fig. 4.4 through Fig. 4.6, we show Mcgarty's result of plotting the function, $10 \log_{10} K(\theta, \phi)$. The effects of shadowing can best be seen by evaluating the total power scattering coefficient ρ_d^2 as function of range, and ρ_d^2 $(= 2 \cdot [\sigma_d^0]^2)$ is given by,

$$\rho_d^2 = \int_0^\pi \int_0^{2\pi} K(\theta, \phi) d\theta d\phi .$$

Figs. 4.7 and 4.8 show $P_r = 10 \log \int_0^\pi \int_0^{2\pi} K(\theta, \phi) d\theta d\phi$
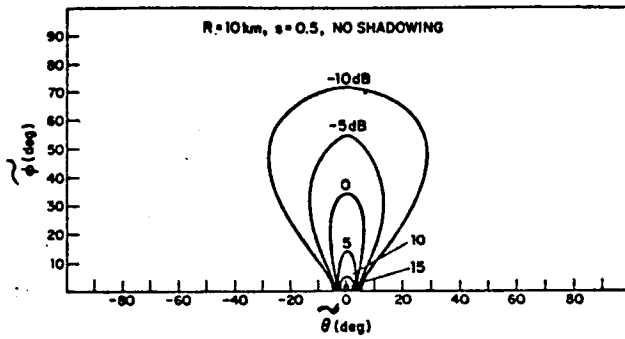
69

Fig. 4.4. CSF with no shadowing.

where, $\tilde{\theta} = \theta - \dfrac{\pi}{2}$, $\tilde{\phi} = \phi - \dfrac{\pi}{2}$, $s = \tan\beta_0$. R = range to emitter
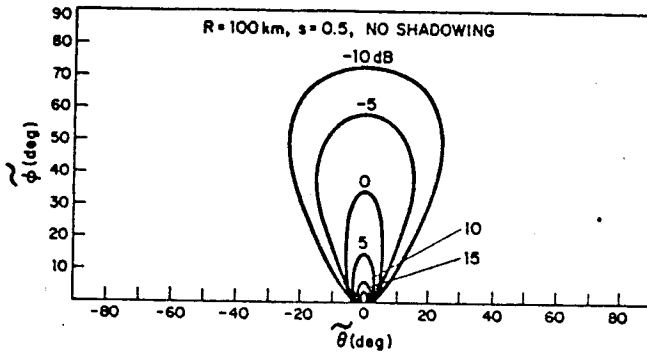

Fig. 4.5. CSF with no shadowing.
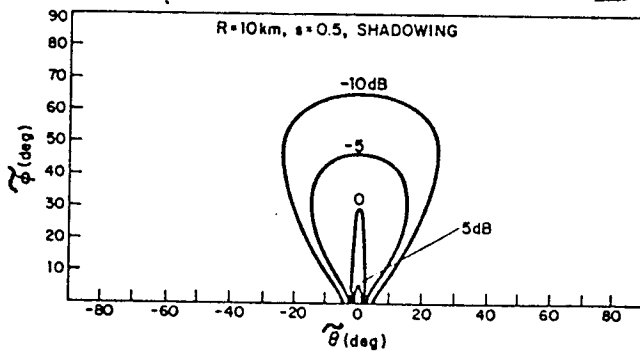
Fig. 4.6. CSF with shadowing
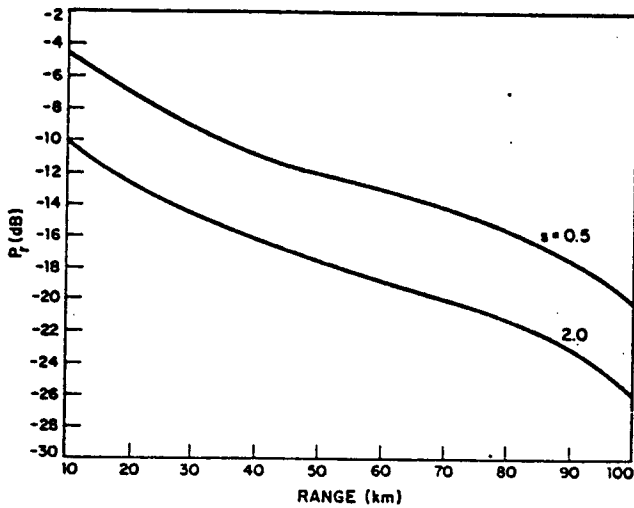
Fig. 4.7. Ratio of diffuse to direct power; shadowing.
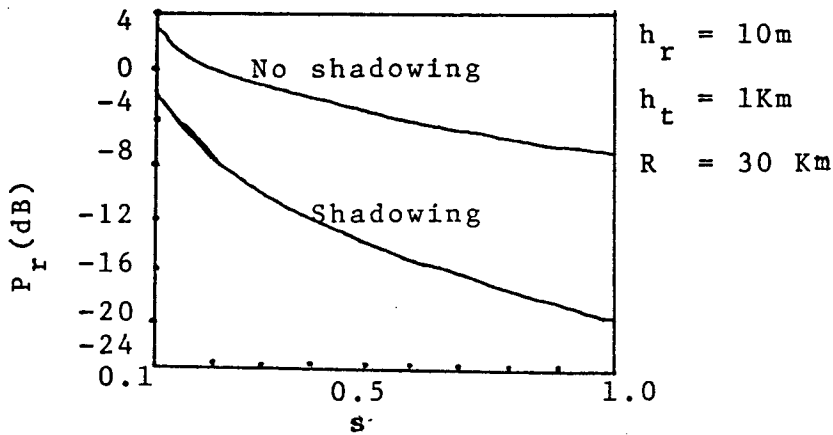
Fig. 4.8. Ratio of diffuse to direct power.

4.4. Sequential likelihood algorithm

The sequential likelihood algorithm proposed, has three versions, depending on whether $\tilde{S}^i(t)$ of Eq. (4.4) is a complex gaussian random process or an unknown function of time.

Let t_i be t in (4.16) for convenience. t can be regarded as a discrete integer index of sequence. From (4.5) and (4.16), the quadrature components obtained at

71

p_3 are,

$$r_R^i(t) = A(t)\cos(\varphi(t) + k_o\mu_1 \cdot d_i) + m_R^i(t) + w_R^i(t)$$

$$r_I^i(t) = A(t)\sin(\varphi(t) + k_o\mu_1 \cdot d_i) + m_I^i(t) + w_I^i(t) \quad (4.21)$$

In this work, the sequential algorithm is to be applied to local range of μ_1, provided that rough estimate of μ_1 is given by simple likelihood statistic based on each observation. Thus the algorithm proposed is essentially a tracking version with validation feature on the rough estimate, μ_1. Firstly, depending on the nature of $\tilde{S}^i(t)$, the corresponding versions of sequential algorithm are given in this section, respectively. Parameter estimation, necessary to implement the algorithm, will be discussed in the next section.

Suppose a rough estimate of μ_1 is given initially by the use of a simple statistic. Then μ_1 range of interest is defined locally, and quantized with step size $\Delta\mu_1$.

$$\mu_1(k) = \mu_{10} + k\Delta\mu; \quad k = o, \pm 1, \pm 2, \ldots \quad (4.22)$$

where μ_{10} is the rough estimate of μ_1 quantized. The estimated lower error bound as well as the degree of complexity allowed will determine the step size $\Delta\mu_1$ in (4.22). From now on, we assume that the situation is such that the effect of quantization error is a secondary one, and further, the emitter of interest is stationary within the kth cell of μ_1 during the several multiples of a processing interval Tp. Thus the set of $\mu_1(k)$ establishes

72

set of hypotheses for the sequential test. We assume an fixed μ_2 for all the hypotheses of $\mu_1(k)$'s.

As a configuration of array, we refer to Fig. 4.9.
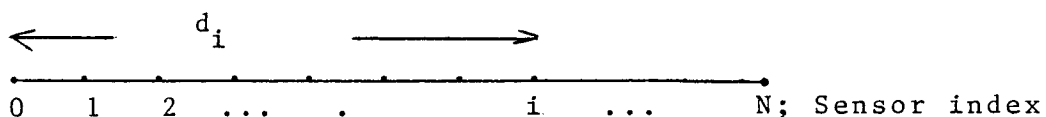
$$t_i = \frac{d_i}{(\frac{\lambda}{2})}; \quad t_i \text{ is integer, } t_o = 0.$$

Fig. 4.9. Configuration of array.

Among the t_i's, at least one pair of them is coprime so as to ensure no inherent ambiguity in the data as explained before. Accordingly, the phase shift term becomes,

$$jk_o\mu_1 \cdot d_i = j2\pi(\frac{d_i}{\lambda})\mu_1 = j2\pi t_i\mu_1. \tag{4.23}$$

CASE 1. When $\tilde{S}_i(t)$ is treated as an unknown function of time with $A^d(t)$ being virtually constant during processing period.

The problem is to find the estimate $\hat{\mu}_1$, maximizing the likelihood function $L_1(\vec{r}(\cdot),\mu_1)$ under the condition that $[A(t),\varphi(t)]$ is unknown function of time. Here $\vec{r}(\cdot)$ represents the set of observations, gathered during n^{th} processing period $[nT_p,(n+1)T_p]$. $\mu_1(k)$'s in (4.22) define the set of hypotheses, H_k's. Observation $\tilde{r}^i(t)$ in complex notation is given from (4.21) as,

$$\tilde{r}^i(t) = A(t)\exp(j\varphi(t))\exp(j2\pi t_i\mu_1) + \tilde{m}^i(t) + \tilde{w}^i(t),$$

$$i = 0,1,2,...,N \tag{4.24}$$

73

Conversion of $\vec{r}(t)$ is required to get rid of the unknown parameter set $[A(t), \varphi(t)]$. The converting procedure under each hypothesis H_k, is given next.

Let the true hypothesis be H_ℓ (i.e., $\mu_1 = \mu_1(\ell)$). Under each H_k, let's define the new observation set , $\{\tilde{y}_k^i(t), i = 1, 2, \ldots, N\}$, as following.

$$\tilde{z}_k^i(t) = \exp(j2\pi t_i \mu_1(k))\}^* \cdot \tilde{r}^i(t); \quad * = \text{complex conjugate}$$

$$\tilde{y}_k^i(t) = \tilde{z}_k^i(t) - \tilde{z}_k^o(t); \quad \tilde{z}_k^o(t) = \tilde{r}^o(t)$$

$$i = 1, 2, \ldots, N, \qquad (4.25)$$

Rewriting $\tilde{y}_k^i(t)$ yields,

$$\tilde{y}_k^i(t) = A(t)\exp(j\varphi(t))[\exp(j2\pi t_i(\mu_1(\ell) - \mu_1(k)) - 1]$$

$$+ [\tilde{m}_i(t)\exp(-j2\pi t_i \mu_1(k)) - \tilde{m}_o(t)]$$

$$+ [\tilde{w}_i(t)\exp(-j2\pi t_i \mu_1(k)) - \tilde{w}_o(t)],$$

$$i = 1, 2, \ldots, N \qquad (4.26)$$

At the true hypothesis H_ℓ, $\tilde{y}_\ell^i(t)$ becomes,

$$\tilde{y}_\ell^i(t) = \tilde{m}_i(t) \cdot \exp(-j2\pi t_i \mu_1(\ell)) - \tilde{m}_o(t)$$

$$+ \tilde{w}_i(t) \cdot \exp(-j2\pi t_i \mu_1(\ell)) - \tilde{w}_o(t)$$

$$i = 1, 2, \ldots, N. \qquad (4.27)$$

In the above, $\tilde{m}_i(t) \cdot \exp(-j2\pi t_i \mu_1(\ell))$ is the diffuse component with its biased phase shift converted. We restate the contents up to now in terms of the real quantities for the purpose of processing, and as a result, we have the expressions (4.28), (4.29) for the observation model.

$$
\begin{bmatrix}
M_R^o(t) \\
M_I^o(t) \\
M_R^1(t) \\
M_I^1(t) \\
\vdots \\
M_R^N(t) \\
M_I^N(t)
\end{bmatrix}
=
\begin{bmatrix}
T_o(k) & & & & \\
& T_1(k) & & & \\
& & \ddots & & \\
& & & \ddots & \\
& & & & T_N(k)
\end{bmatrix}
\begin{bmatrix}
m_R^o(t) \\
m_I^o(t) \\
m_R^1(t) \\
m_I^1(t) \\
\vdots \\
m_R^N(t) \\
m_I^N(t)
\end{bmatrix}
$$

$$
= S(k) \cdot [m_R^1(t), \ m_I^1(t), \ldots, m_R^N(t), m_I^N(t)]^T \qquad (4.28)
$$

where, $M_R^i(t) + j\,M_I^i(t) = \tilde{m}_i(t) \cdot \exp(-j2\pi t_i \mu_1(\ell))$

$S(k)$ is the phase shifting matrix; $S(k)S^T(k) = I_{2(N+1)}$

$$
T_i(k) = \begin{bmatrix}
\cos(2\pi t_i \mu_1(k)), & \sin(2\pi t_i \mu_1(k)) \\
-\sin(2\pi t_i \mu_1(k)), & \cos(2\pi t_i \mu_1(k)).
\end{bmatrix}
$$

Since we are calculating a likelihood function with the assumption that H_k is true, the observation model is given by (4.27).

$$
\begin{bmatrix} y_R^1(t) \\ y_I^1(t) \\ \cdot \\ \cdot \\ \cdot \\ \cdot \\ y_R^N(t) \\ y_I^N(t) \end{bmatrix}
=
\left[\begin{array}{cc|ccccc}
-1, & 0 & 1 & 0 & 0 & & \\
0, & -1 & 0 & 1 & 0 & & \\
-1, & 0 & 0 & 0 & 1 & 0 & 0 \\
0, & -1 & 0 & 0 & 0 & 1 & 0 \\
& & & \cdot & & & \\
& & & \cdot & & & \\
& & & \cdot & & & \\
-1, & 0 & & & & 1 & 0 \\
0, & -1 & & & & 0 & 1
\end{array}\right]
\cdot
\begin{bmatrix} M_R^o(t) \\ M_I^o(t) \\ M_R^1(t) \\ M_I^1(t) \\ \cdot \\ \cdot \\ \cdot \\ M_R^N(t) \\ M_I^N(t) \end{bmatrix}
$$

$$
+
\left[\begin{array}{cc|c}
-1, & 0 & \\
0, & -1 & T_1(k) \\
-1, & 0 & \\
& & T_2(k) \\
& \cdot & \\
& \cdot & \\
& \cdot & \\
& \cdot & \\
-1, & 0 & \\
0, & -1 & T_N(k)
\end{array}\right]
\begin{bmatrix} w_R^o(t) \\ w_I^o(t) \\ w_R^1(t) \\ w_I^1(t) \\ \cdot \\ \cdot \\ \cdot \\ w_R^N(t) \\ w_I^N(t) \end{bmatrix}
\quad (4.29)
$$

where, $y_R^i(t)$ and $y_I^i(t)$ stand for the real and imaginary part of $\tilde{y}_k^i(t)$ respectively. The required covariance matrix is,

$$Q_1(t,s) = E(\vec{M}(t)\vec{M}^T(s))$$

$$E(\vec{w}(t)\vec{w}^T(s)) = \frac{N_o}{2}\delta(t-s)I_{2(N+1)}$$

We can reasonably assume that under the isotropic and homogeneous rough surface, $Q_1(t,s)$ is independent of $\mu_1(k)$, and depends on the parameters of surface, e.t.c. for horizontal

array, given μ_2. In general, $Q_1(t,s)$ may depend on μ_1.

However, since we are observing a data from the given true

$\mu_1(\ell)$, it is not feasible to obtain knowledge of $Q_1(t,s,\mu_1)$.

A sub-optimal processing would be one that assumes the same

$Q_1(t,s)$ for local range of $\mu_1(k)$.

o<u>Algorithm I</u>

1. Under each hypothesis H_k,

    oPerform data conversion from $\vec{r}(t)$.

    oEvaluation $L_1(\vec{y}_k(t), nT_p \le t < (n+1)T_p/\mu_1(k))$ sequentially

    by use of state-space approach [16].

    Here, the likelihood function L_1 is given by,

    $$L_1(\vec{y}_k(t), nTp \le t < (n+1)T_p/\mu_1(k))$$

    $$\triangleq \log f_{pdf}(\vec{y}_k(t), nT_p \le t < (n+1)T_p/\mu_1(k)). \qquad (4.30)$$

2. Select $\hat{k}$ that maximizes $L_1(\vec{y}_k(\cdot)/\mu_1(k))$, and $\mu_1(\hat{k})$

    is the ML estimate.

<u>CASE II</u>. When $\tilde{S}^i(t)$ is treated as a complex gaussian process

during processing period.

As before, the problem is to find the estimate $\hat{\mu}_1$,

maximizing the likelihood function $L_2(\vec{r}(t), nT_p \le t < (n+1)T_p/\mu_1(k))$

under the condition that $\tilde{S}^i(t)$ is a gaussian process.

The observation model is given by (4.21), where the

quadratures of signal part are an i.i.d. pair of gaussian

processes under each H_k.

The joint observation set under hypothesis H_k is

77

$$
\begin{bmatrix} r_R^o(t) \\ r_I^o(t) \\ \cdot \\ \cdot \\ \cdot \\ \cdot \\ \cdot \\ r_R^N(t) \\ r_I^N(t) \end{bmatrix} = \begin{bmatrix} T_o^{-1}(k) \\ \cdot \\ \cdot \\ \cdot \\ \cdot \\ \cdot \\ \\ \\ T_N^{-1}(k) \end{bmatrix} \cdot \begin{bmatrix} A(t)\cos\varphi(t) \\ A(t)\sin\varphi(t) \end{bmatrix} + \begin{bmatrix} m_R^o(t) \\ m_I^o(t) \\ \cdot \\ \cdot \\ \cdot \\ \\ m_R^N(t) \\ m_I^N(t) \end{bmatrix}
$$

$$
+ \begin{bmatrix} w_R^o(t) \\ w_I^o(t) \\ \cdot \\ \cdot \\ \cdot \\ \cdot \\ w_R^N(t) \\ w_I^N(t) \end{bmatrix} \tag{4.31}
$$

where $T_i^{-1}(k) = \begin{bmatrix} \cos(k_o \mu_1(k) \cdot d_i), & -\sin(k_o \mu_1(k) \cdot d_i) \\ \sin(k_o \mu_1(k) \cdot d_i), & \cos(k_o \mu_1(k) \cdot d_i) \end{bmatrix}$, $T_o(k) = I$.

Rearranging (4.31) yields,

78

$$
\begin{bmatrix} r_R^0(t) \\ r_I^0(t) \\ \cdot \\ \cdot \\ \cdot \\ \cdot \\ r_R^N(t) \\ r_I^N(t) \end{bmatrix}
=
\left[\begin{array}{c:c} \begin{matrix} T_0^{-1}(k) \\ T_1^{-1}(k) \\ \cdot \\ \cdot \\ \cdot \\ \\ \\ T_N^{-1}(k) \end{matrix} & I_{2(N+1)} \end{array}\right]
\cdot
\begin{bmatrix} S_1(t) \\ S_2(t) \\ \hdashline m_I^0(t) \\ m_I^0(t) \\ \cdot \\ \cdot \\ \cdot \\ m_R^N(t) \\ m_I^N(t) \end{bmatrix}
+
\begin{bmatrix} w_R^0(t) \\ w_I^0(t) \\ \cdot \\ \cdot \\ \cdot \\ \\ w_R^N(t) \\ w_I^N(t) \end{bmatrix}
$$

From (4.28),

$$
=
\left[\begin{array}{c:c} \begin{matrix} T_0^{-1}(k) \\ T_1^{-1}(k) \\ \\ \\ \\ \\ \\ \\ T_N^{-1}(k) \end{matrix} & S^T(k) \end{array}\right]
\cdot
\begin{bmatrix} S_1(t) \\ S_2(t) \\ M_R^0(t) \\ M_I^0(t) \\ \cdot \\ \cdot \\ M_R^N(t) \\ M_I^N(t) \end{bmatrix}
+
\begin{bmatrix} w_R^0(t) \\ w_I^0(t) \\ \cdot \\ \\ \cdot \\ \\ w_R^N(t) \\ w_I^N(t) \end{bmatrix}
\qquad (4.32)
$$

where, $S_i(t) = A(t) \begin{bmatrix} \cos\varphi(t) \\ \sin\varphi(t) \end{bmatrix}$ is the quadratures of the combined signal part observed at the 0th reference channel.

The required covariance matrix is,

$$Q_2(t,s) = \begin{bmatrix} E(S_1(t)S_1(S)) & 0 & \\ & & 0 \\ 0 & E(S_2(t)S_2(S)) & \\ \hline & & \\ & 0 & \\ & & E(M(t)M(S)^T) \end{bmatrix}$$

$$E(\vec{w}(t)\vec{w}^T(s)) = \frac{N_o}{2} \cdot \delta(t-s) \cdot I_{2(N+1)}$$

From (4.32), the sequential algorithm for this case is the following:

Algorithm II

1. Under each hypothesis H_k, the observation model is defined by (4.32).

    Evaluate $L_2(\vec{r}(t), nT_p \leq t < (n+1)T_p / \mu_1(k))$ sequentially, based on the observation model (4.32) by use of state space approach.

    Here, the likelihood function L_2 is given by,

    $$L_2(\vec{r}(t), nT_p \leq t < (n+1)T_p / \mu_1(k))$$

    $$\overset{\Delta}{=} \log \frac{f_{pdf}(\vec{r}(t), nT_p \leq t < (n+1)T_p / \mu_1(k))}{f_{pdf}(\vec{r}(t), nT_p \leq t < (n+1)T / H_{NULL})} \qquad (4.33)$$

2. Select $\hat{k}$ that maximizes $L_2(\vec{r}(\cdot), \mu_1(k))$, and $\mu_1(\hat{k})$ is the ML estimate.

    In (4.33), after $\mu_1(\hat{k})$ is selected, $L_2(\mu_1(\hat{k}))$ can be used for the detection purpose with some present value Λ_o. Pattern of $L_i(\mu_1(k))$ over k may also be processed for the

detection purpose.

<u>CASE III</u>

When $\tilde{\vec{s}}^i(t)$ is treated as a constant, during processing period.

This situation corresponds to the case when the emitter of interest is relatively stationary in all the aspects. The problem is to find the estimate $\hat{\mu}_1$, maximizing the likelihood function $L_3(\vec{r}(t), nT_p \leq t < (n+1)T_p/\mu_1(k))$ under the condition that $\tilde{\vec{s}}^i(t)$ is a constant. The joint observation set under each H_k is given by (4.31), where $\{A(t)\cos\varphi(t), A(t)\sin\varphi(t)\}$ are constants during processing period.

<u>Algorithm III</u>

1. Under each hypothesis H_k, the observation model is defined by (4.31). Evaluate $L_3(\vec{r}(t), nT_p \leq t < (n+1)T_p, \mu_1(k))$ sequentially by state space approach.

   Here, $L_3(\vec{r}(t), t \in N_{T_p}, \mu_1(k))$

$$\triangleq \log \frac{f_{pdf}(\vec{r}(t), t \in N_{T_p}/\mu_1(k))}{f_{pdf}(\vec{r}(t), t \in N_{T_p}/H_{NULL})} \qquad (4.34)$$

As an approximate way to obtain ($A \cos\varphi$, $A \sin\varphi$), integration of the each quadratures ($r_R^o(t)$, $r_I^o(t)$) at the reference sensor is performed during processing period. Delay of data is required to obtain the sampled mean of quadratures.

2. Select $\hat{k}$ maximizing $L_3(k)$, and $\hat{\mu}_1(k)$ is the ML estimate.

4.5 <u>State space model of signal and diffuse component</u>

We will refer to the observed signal model in Section 4.2 throughout this section. First order discrete gauss-Markov model is used for all the random processes involved,

due to practical limitations. Also random processes are assumed to be locally-stationary as before. Firstly the signal part, if gaussian processes, is modelled as,

$$
\begin{bmatrix} S_1(t+1) \\ S_2(t+1) \end{bmatrix} = \begin{bmatrix} a_1, & 0 \\ 0, & a_1 \end{bmatrix} \begin{bmatrix} S_1(t) \\ S_2(t) \end{bmatrix} + \begin{bmatrix} e_1(t) \\ e_2(t) \end{bmatrix} \tag{4.35}
$$

where quadratures $S_1(t)$, $S_2(t)$ are i.i.d. low-pass processes in steady-state. The diffuse part can also be modelled, using the same format.

The state-space model of joint diffuse component is

$$
\begin{bmatrix} M_R^0(t+1) \\ M_I^0(t+1) \\ \cdot \\ \cdot \\ \cdot \\ M_R^N(t+1) \\ M_I^N(t+1) \end{bmatrix} = a_2 \cdot I_{2(N+1)} \cdot \begin{bmatrix} M_R^0(t) \\ M_I^0(t) \\ \cdot \\ \cdot \\ \cdot \\ M_R^N(t) \\ M_I^N(t) \end{bmatrix} + \begin{bmatrix} d_R^0(t) \\ d_I^0(t) \\ \cdot \\ \cdot \\ \cdot \\ d_R^N(t) \\ d_I^N(t) \end{bmatrix} \tag{4.36}
$$

$M_{R,I}^i(t)$, as defined in (4.28), is an identical low-pass process at each (i, R, I). Also, (M_R^i, M_I^i) is pairwise i.i.d. at each i.

To implement the sequential maximum likelihood algorithm of Section 4.4, we need to know the parameters of underlying random processes. From the reference model (4.35), (4.36), a straight-forward problem statement is to estimate the following parameters from the given observations.

1. a_1

2. a_2

3. $\text{var}[e_i(t)]$

4. $\text{Var}[d_p^i(t)]$, $p = R$ or I

5. Spatial covariance Matrix, $\text{Cov}(\vec{d}(t), \vec{d}(t))$

The observation model (4.29) and the state space model of joint diffuse component (4.36) describe the estimation problem of the underlying parameters for the Case 1, and also the models (4.32), (4.35), (4.36) are for the Case II. Since the observation models depend on $\mu_1(t)$ in all three cases of Section 4.4, the current parameter estimation, using the joint observation, can only be performed aposteriori, and will be used for the next processings. This approach is reasonable, provided that the parameters involved are slowly changing and also a sufficiently correct $\hat{\mu}_1$ is given. The parameters except $\text{Cov}(\vec{d}(t), \vec{d}(t))$ may be estimated at each sensor output, since these are not parameters of joint character.

Depending on the complexity allowed, various kinds of the estimation schemes and a proper simplication on the $\text{Cov}(\vec{d}(t), \vec{d}(t))$ can be employed, ranging from a simple approximate measurements to a sequential estimate of underlying parameters.

4.6 Implementation of the Algorithm III

In this section, we will proceed with Case III under some assumption on the spatial covariance matrix, $\text{Cov}(\vec{M}(t), \vec{M}(t))$.

83

From the diffuse component model in Section 4.2,

$$\tilde{S}_D^i(t) = A^d(t) \int_{-1}^{1}\int_{-1}^{1} M^i(\vec{\mu},\vec{\mu}',t) \exp(jk_o\mu_1'\cdot d_i)\, d\mu_2'\, d\mu_1' \quad (4.16)$$

$$E(\tilde{S}_D^i(t)\tilde{S}_D^{j*}(t))$$

$$= [A^d(t)]^2 \int_{-1}^{1}\int_{-1}^{1} f_{i,j}(\vec{\mu},\vec{\mu}',0) \exp(jk_o\mu_1'(d_i-d_j)\, d\mu_2'\, d\mu_1';$$

where $f_{i,j}(\vec{\mu},\vec{\mu}',0) = E(M^i(\vec{\mu},\vec{\mu}',t)M^j(\vec{\mu},\vec{\mu}';t)*)$ from (4.6)

$$= K(\vec{\mu},\vec{\mu}') \qquad \text{for } i = j$$

$$= [A^d(t)]^2 \int_{-1}^{1}\int_{-1}^{1} K(\vec{\mu},\vec{\mu}')\, d\mu_2'\, d\mu_1' \qquad \text{for } i = j$$

$$= [A^d(t)]^2\, 2\cdot\sigma_d^2.$$

From the above form of correlation, the following compensating factor is set from a macroscopic point of view.

$$E(\tilde{S}_D^i(t) S_D^j(t)*)$$

$$= [A^d(t)]^2 \int_{-1}^{1}\int_{-1}^{1} K(\vec{\mu},\vec{\mu}') \exp(jk_o\mu_1'(d_i-d_j)\, d\mu_2'\, d\mu_1'.$$

$$\cdot \exp(-(d_i-d_j)^2/\ell_f^2).$$

Here, ℓ_f is the characteristic spatial correlation distance of the observed diffuse component. ℓ_f is locally defined within the aperture dimension, and depends on the given geometry of emitter and the statistical properties of rough surface. In a linear horizontal interferometer, ℓ_f is assumed to be locally independent of μ_1, given μ_2. Distribution of the diffuse power along μ_1', $\int_{-1}^{1} K(\vec{\mu},\vec{\mu}')\, d\mu_2'$, can be approximated to be locally even around μ_1, source direction in many cases.

Let μ_1' be $\mu_1 + \Delta_1'$.

$$E(\tilde{S}_D^i(t)\tilde{S}_D^j(t)*)$$

$$= [A^d(t)]^2 \exp(jk_0\mu_1(d_i-d_j))[\int_{-w}^{w}\int_{-1}^{1}K(\vec{\mu},\vec{\mu}')\exp(jk_0\Delta_1'(d_i-d_j))$$

$$d\mu_2'd\Delta_1' \cdot \exp(-(d_i-d_j)^2/\ell_f^2)]$$

(bracketed term is a real quantity), where w is the spread width of Δ_1' determined from the criterion on the power level of $K(\vec{\mu},\vec{\mu}')$, and depends on the source direction $\vec{\mu}$.

$$E(\tilde{S}_D^i(t)\cdot\tilde{S}_D^j(t)*)$$

$$= E(m_R^i(t) + jm_I^i(t))(m_R^j(t) - jm_I^j(t))$$

$$= \exp(jk_0\mu_1(d_i-d_j))\cdot E[M_R^i(t) + jM_I^i(t))(M_R^j(t) - jM_I^j(t))].$$

From the arguments made so far, it is reasonable to assume the following

$$E(M_R^i(t)M_R^j(t)) = E(M_I^i(t)M_I^j(t))$$

$$= \frac{1}{2} \cdot [A^d(t)]^2 \int_{-w}^{w}\int_{-1}^{1}K(\vec{\mu},\vec{\mu}')\exp(j\ k_0\ \cdot\ \Delta_1'\ \cdot\ (d_i-d_j))d\mu_2'd\mu_1'$$

$$\cdot \exp(-d_i-d_j)^2/\ell_f^2$$

$$E(M_R^i(t)M_I^j(t)) = E(M_I^i(t)M_R^j(t)) = 0. \qquad (4.38)$$

Equation (4.38) defines $\text{Cov}(\vec{M}(t),\ \vec{M}(t))$ in theory in the presence of spatially dispersive channel, based on the CSF and the spatial correlation distance ℓ_f.

A simpler form of processor can be obtained by using unspread channel approach in the presence of spatially dispersive channel, in which case spatial correlation factor, $\exp[-(d_i-d_j)^2\ell_f^2]$, is to be disregarded. (T.P. Mcgarty, [12]).

We will take a different simplification by taking the

85

advantage of horizontal interferometer; the CSF $K(\vec{\mu},\vec{\mu}')$ is relatively concentrated around μ_1. Thus the following approximation is taken.

$$\int_{-w}^{w}\int_{-1}^{1} K(\vec{\mu},\vec{\mu}')\ \exp(jk_o \cdot \Delta_1' \cdot (d_i - d_j)\,d\mu_2'\,d\Delta_1'$$

$$\cong \int_{-w}^{w}\int_{-1}^{1} K(\vec{\mu},\vec{\mu}')\cdot 1 \cdot d\mu_2'\,d\Delta_1' = 2\cdot\sigma_d^2. \qquad (4.39)$$

When $k_o \cdot w \cdot d_N \ll 1$, (4.39) is perfectly correct. According to (4.39), the qualitative behavior of the diffuse component lies between those of the specular and the RCVR noise, and thus the effect of the direction spread is not treated explicitly other than a contribution of power in the linear horizontal array.

The simplified covariance matrix $\text{Cov}(\vec{M}(t),\vec{M}(t)]$ is given by,

$$\text{Cov}[\vec{M}(t),\vec{M}(t)]$$

$$= \frac{[A^d(t)]^2 \cdot \sigma_d^2}{D^2} \begin{bmatrix} 1 & 0 & \Delta_{12} & 0 & & \Delta_{1N'} & 0 \\ 0 & 1 & 0 & \Delta_{12} & & 0, & \Delta_{1,N} \\ \Delta_{21}, & 0, & 1 & 0 & & & \\ 0, & \Delta_{21}, & 0 & 1 & & & \\ \Delta_{N,1,0} & & & & & 1 & 0 \\ 0, & \Delta_{N,1} & & & & 0 & 1 \end{bmatrix} \qquad (4.40)$$

, where $\Delta_{i,j} = \exp((d_i - d_j)^2/\ell_f^2)$.

From the state space model of the diffuse component (4.36),

$$\text{Cov}(\vec{M},\vec{M}) = a_2^2 \, \text{Cov}(\vec{M},\vec{M}) + \text{Cov}(\vec{d},\vec{d})$$

$$\text{Cov}(\vec{d},\vec{d}) = (1 - a_2^2)\text{Cov}(\vec{M},\vec{M}) \tag{4.41}$$

Under each hypothesis H_k in Case III, the following models are the relevant ones.

$$
\begin{bmatrix} M_R^0(t+1) \\ M_I^0(t+1) \\ \cdot \\ \cdot \\ \cdot \\ M_R^N(t+1) \\ M_I^N(t+1) \end{bmatrix}
= a_2 \begin{bmatrix} & & \\ & I_{2(N+1)} & \\ & & \end{bmatrix}
\begin{bmatrix} M_R^0(t) \\ M_I^0(t) \\ \cdot \\ \cdot \\ \cdot \\ M_R^N(t) \\ M_I^N(t) \end{bmatrix}
+ \begin{bmatrix} d_R^0(t) \\ d_I^0(t) \\ \cdot \\ \cdot \\ \cdot \\ d_R^N(t) \\ d_I^N(t) \end{bmatrix}
$$

$$
\underbrace{\left\{ \begin{bmatrix} r_R^0(t) \\ r_I^0(t) \\ \cdot \\ \cdot \\ \cdot \\ r_R^N(t) \\ r_I^N(t) \end{bmatrix}
- \begin{bmatrix} T_0^{-1}(k) \\ \\ \\ \\ T_N^{-1}(k) \end{bmatrix} \right\}}_{\triangleq\; z^k(t)}
\cdot \begin{bmatrix} S_1 \\ S_2 \end{bmatrix}
= \begin{bmatrix} S^T(k) \end{bmatrix}
\underbrace{\left\{ \begin{bmatrix} M_R^0(t) \\ M_I^0(t) \\ \cdot \\ \cdot \\ \cdot \\ M_R^N(t) \\ M_I^N(t) \end{bmatrix}
+ \begin{bmatrix} w_R^0(t) \\ w_I^0(t) \\ \cdot \\ \cdot \\ \cdot \\ w_R^N(t) \\ w_I^N(t) \end{bmatrix} \right\}}_{\triangleq\; S_M^k(t)}
$$

Under the null hypothesis H_{NULL},

$$
\begin{bmatrix} r_R^0(t) \\ r_I^0(t) \\ \cdot \\ \cdot \\ \cdot \\ r_R^N(t) \\ r_I^N(t) \end{bmatrix} = \begin{bmatrix} w_R^0(t) \\ w_I^0(t) \\ \cdot \\ \cdot \\ \cdot \\ w_R^N(t) \\ w_I^N(t) \end{bmatrix}
$$

The above set defines the system matrices for Kalman filtering to evaluate likelihood function sequentially. Let's assume that the parameter set $[D, a_2, \ell_f, N_o]$ is estimated from the previous data, and thus write down the equations necessary for the sequential evaluation of likelihood function.

$$
L_3(t/\mu_1(k)) = \log\{f_{pdf}(\vec{z}^k(t), t\epsilon NT_p)\}
$$

$$
- \log\{f_{pdf}(\vec{r}(t)/H_{NULL})\}
$$

$$
\triangleq \lambda_1(t,k) - \lambda_2(t).
$$

From now on, the index k as well as the vector notation "→" will be omitted whenever the meaning is clear.

From Schweppe's formula [16],

$$
2[\lambda_1(t) - \lambda_1(t-1)]
$$

$$
= - \log(2\pi)^{2(N+1)} |\Sigma_z(t/t-1)| - q^T(t)\Sigma_z^{-1}(t/t-1)q(t) \quad (4.42)
$$

where,

$$
q(t) = z(t) - \hat{z}(t/t-1)
$$

$$= z(t) - \hat{S}_M(t/t-1) = z(t) - S^T(k)\hat{M}(t/t-1)$$

Let's denote the first sequence in every N^{th} processing period as $t = 0$ for convenience. T_p sequences are taken during each period. Then, in (4.42), the initial conditions are given by,

$$\left. \begin{array}{l} q(0) = z(0) \\[1em] \lambda_1(-1) = 0 \\[1em] \Sigma_z(0/-1) = E(z(0)z^T(0)) \\[1em] = S^T(k)\text{Cov}(\vec{M}(0), \vec{M}(0))S(k) + \dfrac{N_o}{2} I_{2(N+1)} \end{array} \right] \qquad (4.43)$$

$\text{Cov}(\vec{M}(0), \vec{M}(0))$ is steady-state covariance matrix.

Kalman filtering equation is,

$$\left. \begin{array}{l} \hat{M}(t+1/t) = a_2 \cdot \hat{M}(t/t-1) + K(t)\{z(t) - S^T(k)\hat{M}(t/t-1)\} \\[1em] \hat{M}(0/-1) = 0. \end{array} \right.$$

The gain matrix $K(t)$ is given by,

$$\left. \begin{array}{l} K(t) = a_2 \cdot P(t)S(k)[S^T(k)P(t)S(k) + R_2]^{-1} \\[1em] R_2 = \dfrac{1}{2} N_0 \ I_{2(N+1)} \end{array} \right] \qquad (4.44)$$

where error covariance matrix $P(t)$ is,

$$\begin{array}{l} P(t+1) = a_2 \cdot [a_2 I_{2(N+1)} - K(t)S^T(k)]P(t) + R_1 \\[1em] R_1 = \text{cov}(\vec{d}(0), \vec{d}(0)) = (1 - a_2^2)\text{cov}(\vec{M}(0), \vec{M}(0)) \\[1em] P(0) = \text{cov}(\vec{M}(0), \vec{M}(0)). \end{array}$$

In (4.42), $\Sigma_z(t/t-1) = P(t) + \dfrac{N_o}{2} I$. $\lambda_1(t)$ is sequentially evaluated by use of $\hat{M}(t/t-1)$ from Kalman filtering.

$$2(\lambda_2(t) - \lambda_2(t-1))$$

$$= -\log(N_o \pi)^{2(N+1)} - \frac{2}{N_o} r^T(t) \cdot r(t)$$

with $\lambda_2(-1) = 0$.   (4.45)

Thus, the recursive equation for $L_3(t,k)$ is,

$$2\{L_3(t,k) - L_3(t-1,k)\}$$

$$= 2\{\lambda_1(t,k) - \lambda_1(t-1,k)\} - 2\}\lambda_2(t) - \lambda_2(t-1)\}$$

$$= -\log(2\pi)^{2(N+1)} |\Sigma_z(t/t-1)| - q^T \Sigma_z^{-1}(t/t-1)q(t)$$

$$+\log(N_o \pi)^{2(N+1)} + \frac{2}{N_o} r^T(t) \cdot r(t).$$

$$= \log(\frac{N_o}{2})^{2(N+1)} - \log|\Sigma_z(t/t-1)| + \{\frac{2}{N_o} r^T(t) \cdot r(t)$$

$$-q^T(t) \Sigma_z^{-1}(t/t-1)q(t)\}$$ (4.46)

Equations (4.42)-(4.46) define $L_3(t,k)$, once
$[a_2, \text{Cov}(\vec{M}(0), \vec{M}(0))]$ is given uder the first order state-space
model of $\vec{M}(t)$. In turn, $\text{Cov}(\vec{M}(0), \vec{M}(0))$ depends on $[D, \ell f, a_2]$
under the simplified covariance matrix model of (4.40).

As a possible simplification, one can think of the
following.

   1. Use of the steady-state Kalman gain matrix, during
       each processing period.

   2. $s^T(k) \to s^T(0)$, since local region of μ_1 is
       interested in tracking version, where $\mu_1(0)$ is
       being updated with $\mu_1(0) = \hat{\mu}_1(T_p)$. With $s^T(k) =$
       $s^T(0)$, $\Sigma_z(t/t-1)$ is independent of hypothesis H_k
       assumed.

The remaining future area is to obtain an alternative
way of updating $(a_2, \text{Cov}(\vec{M}(0), \vec{M}(0))$ by a feedback-type

adaptation.

As for the future analysis, the following ones are important:

1. Sensitivity of the sequential ML estimate $\hat{\mu}_1$ on the underlying parameters involved.

2. Justification of the use of first-order state-space model, as far as $\hat{\mu}_1$ is concerned.

3. Analysis of direction spread effect by some practical parameter.

In summary, the exact block diagram is drawn for the sequential processing of case III.
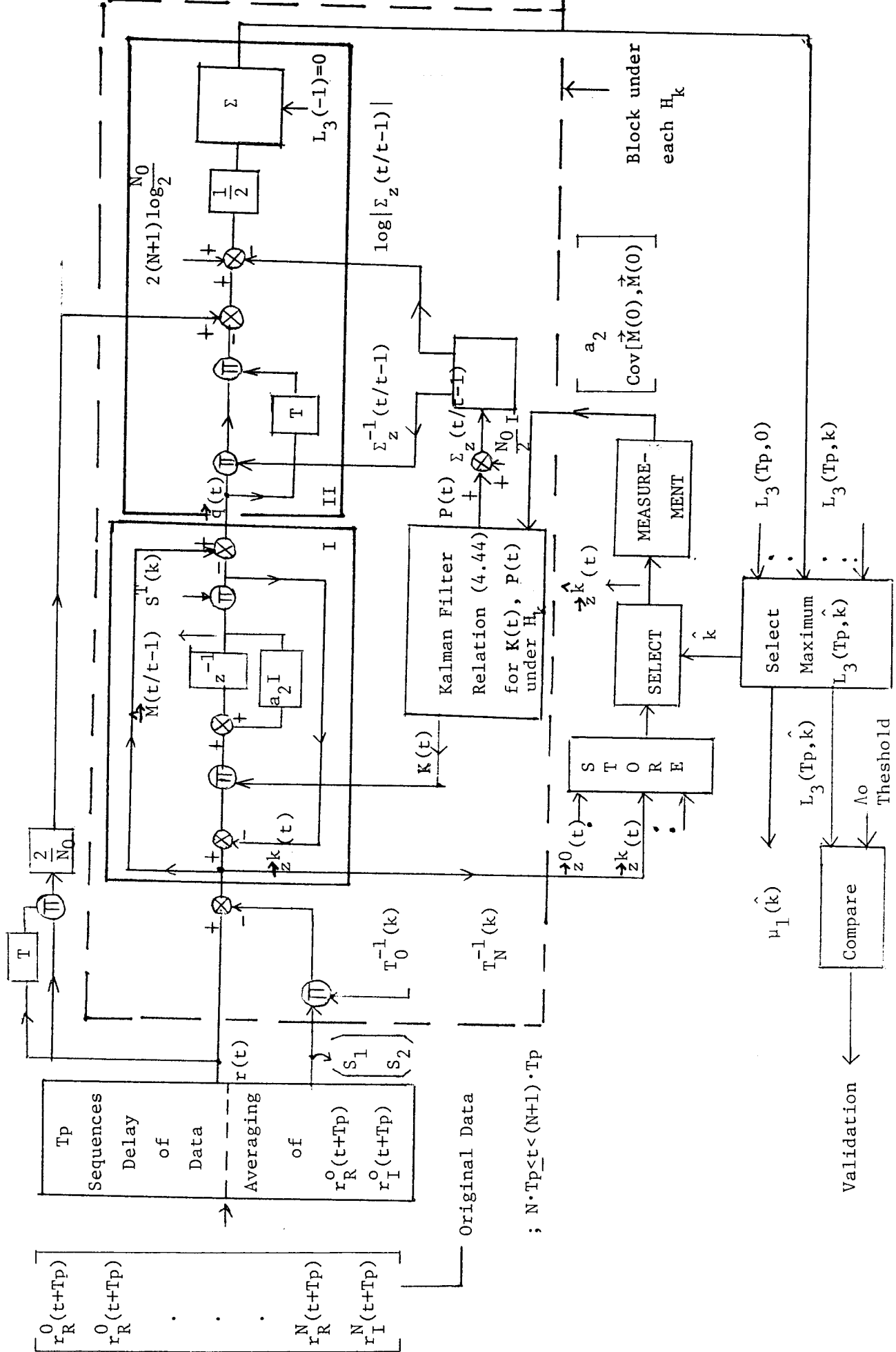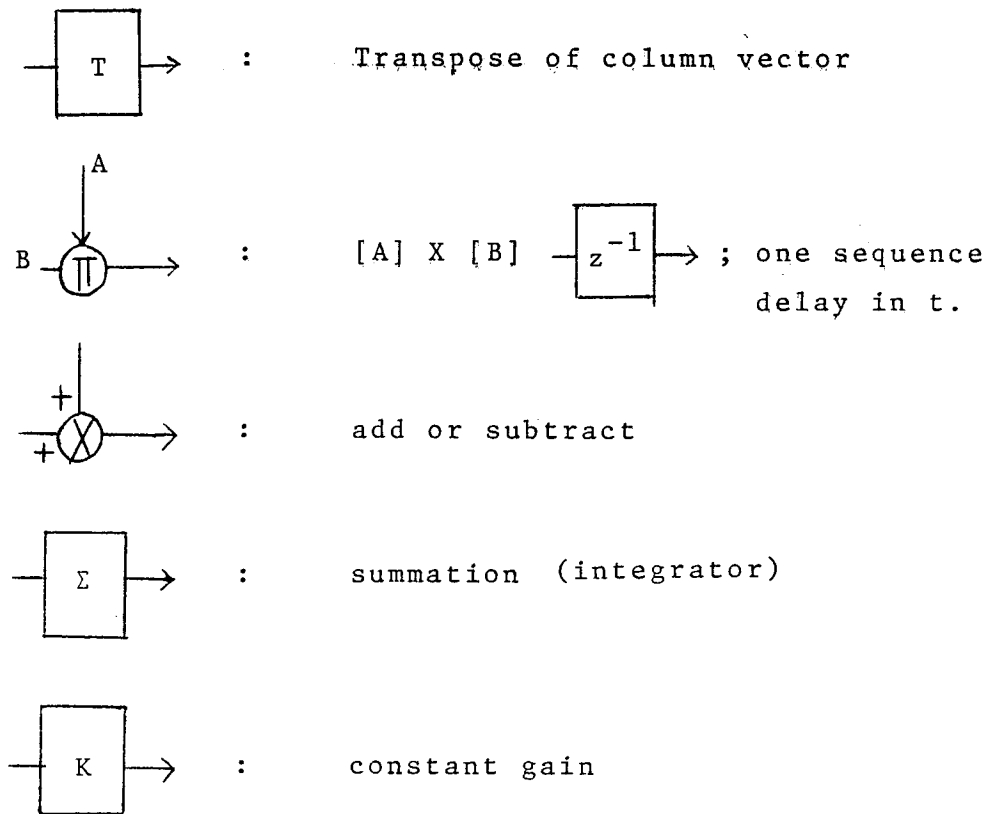
Fig. 4.10. Block diagram of the processor for Case III

92

In Fig. 4.4, the following conventions are used:

[T] ⟶   :   Transpose of column vector

B ⟶(π)⟶ (with A input) : [A] X [B]   [z⁻¹]⟶ ; one sequence delay in t.

⟶(X)⟶ (with + inputs) : add or subtract

[Σ]⟶   :   summation (integrator)

[K]⟶   :   constant gain

subblock I   :   Kalman filter under each H_k

subblock II   :   likelihood calculator under each H_k.

4.7. Simplified algorithm

In this section, we will extend the statistic described in Section 3.3, Case III. The same receiver configuration of Fig. 4.2 will be used except the following replacement of the common reference signal (IF) as given below.

IF Output from the 1st Sensor

IF Output from the ref. Sensor
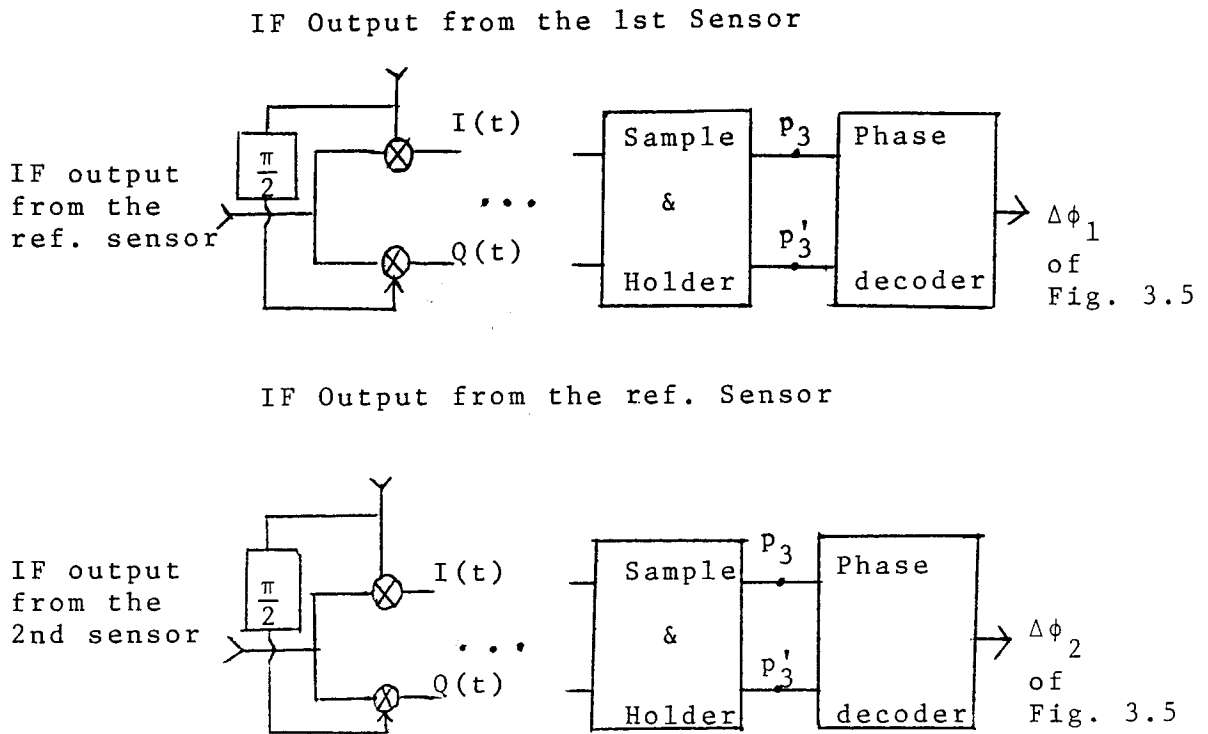

Fig. 4.11.   Receiver configurations for
             Midphase of Case III.

With dynamics of emitter relatively in a wide range,

one can assume that the emitter is within the given ambiguity

lobe during a processing period T_p. T_p will be determined

by the range to the emitter.

As a simplified version of algorithms described in the

previous sections of this chapter, a sequential hypothesis

test will be given to the ambiguity lobe (k_1, k_2) of Section

3.3.   The algorithm to be described is a combination of a

sequential hypothesis test with the usual statistic based on

each observation for the fine resolution of sin θ.   The

94

objective of this approach is to enhance the performance of ambiguity resolution, given the specification of error in the fine resolution.

First assumption on the observed signal model is that the diffuse component can be approximated to an independent process from sample to sample. The above situation may be expected to arise in practice when the spectrum of diffuse component is wide, due to a large tangential velocity of the emitter, (tangential to the ground), or when other rapidly fluctuating factors are involved.

Let the IF outputs from each sensor be $x_i(t)$'s.

$$\left.\begin{aligned}
x_0(t) &= (A(t) + m_0^1(t) + w_0^1(t))\cos(\omega t + \varphi(t)) \\
&\quad + (m_0^2(t) + w_0^2(t))\sin(\omega t + \varphi(t)) \\
x_1(t) &= (A(t) + m_1^1(t) + w_1^1(t))\cos(\omega t - p\pi v(t) + \varphi(t)) \\
&\quad + (m_1^2(t) + w_1^2(t))\sin(\omega t - p\pi v(t) + \varphi(t)) \\
x_2(t) &= (A(t) + m_2^1(t) + w_2^1(t))\cos(\omega t + q\pi v(t) + \varphi(t)). \\
&\quad + (m_2^2(t) + w_2^2(t))\sin(\omega t + q\pi v(t) + \varphi(t))
\end{aligned}\right\} \quad (4.47)$$

$v(t) = \sin\theta(t)$: $\theta(t)$ is the angle from the normal to the axis of array as in Fig. 3.5.

$m_i^p(t)$: quadratures of the diffuse component at the ith sensor with variance σ_D^2

$w_i^p(t)$: quadratures of the receiver noise at the ith sensor with variance σ_R^2.

By use of integrator in the configuration of the

95

receiver, we can re-define the observation properly as in
the case of Eqs. (4.13) or (4.16). Thus from now on, we
will neglect the notational complexity. As a note, we
mention the followings in connection with the above represent-
ation of $x_i(t)$'s.

(1) $\cos\omega t$ is reference signal in mind, and is used
     as phase reference.

(2) $A(t)\cos(\omega t + \varphi(t))$ is the combination of the
     direct component and specular component.

(3) Receiver noise is originally represented by $w(t) = $
     $w^{1'}(t)\cos\omega t + w^{2'}(t)\sin\omega t$. Representation of
     the form $w^1(t)\cos(\omega t + \varphi(t)) + w^2(t)\sin(\omega t + \varphi(t))$
     is related to $(w^{1'}(t), w^{2'}(t))$ by the orthogonal
     transformation, which preserves independence
     between the quadratures.

$$
\begin{bmatrix} w^1(t) \\ w^2(t) \end{bmatrix} = \begin{bmatrix} \cos\varphi(t), & -\sin\varphi(t) \\ \sin\varphi(t), & \cos\varphi(t) \end{bmatrix} \cdot \begin{bmatrix} w^{1'}(t) \\ w^{2'}(t) \end{bmatrix} \tag{4.48}
$$

Due to the white property of $w^{i'}(t)$, the correlation of
$w^i(t)$ is the same as that of $w^{i'}(t)$ for any sample path $\varphi(t)$.
Thus the statistical property of (w^1, w^2) is the same as
that of $(w^{1'}, w^{2'})$, and only sample values are different.
Same arguments hold for $\varphi(t) + p\pi \sin\theta(t)$, and also for $m_i^p(t)$.

From Equation (3.33) which corresponds to $x_i(t)$'s and
the observation model (3.35), the observation $(\Delta\phi_1, \Delta\phi_2)$ at
p_3 of Fig. 4.11 is given by

96

$$\Delta\phi_1(t) = p\pi v + \frac{1}{A(t)}(m_1^2(t) - m_o^2(t) + w_1^2(t) - w_o^2(t)) - 2\pi k_1$$

$$= p\pi v + \Delta\phi_\varepsilon^1(t) - 2\pi k_1$$

$$\Delta\phi_2(t) = q\pi v + \frac{1}{A(t)}(-m_2^2(t) + m_o^2(t) - w_2^2(t) + w_o^2(t)) - 2\pi k_2$$

$$= q\pi v + \Delta\phi_\varepsilon^2(t) - 2\pi k_2$$

$$(4.49)$$

where (p, q) is a coprime pair of integers as before.

We assume one emitter under homogeneously rough surface. Under this environment, $\frac{\sigma_D^2}{A^2}$ is usually less than 0.1, considering Fresnel reflection coefficient. Consequently, $\frac{1}{A^2}(\sigma_D^2 + \sigma_R^2)$ is less than 0.2 with $\frac{\sigma_R^2}{A^2} < 0.1$. Therefore, we may expect that the In-phase components are not important, and thus we obtain the observation model (4.49) for elevation greater than 5°. The restriction on the range of elevation is necessary to ensure above ratios, considering the cancelling effect of the specular component.

Also the amplitude of signal $A(t)$ is assumed to be slowly fluctuating, so that we can treat $A(t)$ virtually constant during the processing period T_p. Hence we may treat $(\Delta\phi_\varepsilon^1(t), \Delta\phi_\varepsilon^2(t))$ as stationary, independent process during the processing period T_p (i.e., power of the diffuse component will not be varying much, due to the limitation of the emitter dynamics). Provision to reject an abnormally low value of $A(t)$ is to be made, since data is then meaningless. Also we assume that spatial covariances of $m_i^p(t)$'s are independent of θ.

97

By using the statistic based on each observation, the fine resolution estimate $v_{k_1,k_2}(t)$ is given from Eq. (3.38) by

$$v_{k_1,k_2}(t) = \sin\hat{\theta}]_{k_1,k_2} = \pi([p,q]P^{-1}\begin{bmatrix} p \\ q \end{bmatrix})^{-1}[p,q]P^{-1}\begin{bmatrix} \Delta\phi_1(t)+2\pi k_1 \\ \Delta\phi_2(t)+2\pi k_2 \end{bmatrix}$$

Covariance matrix P should be $E[\Delta\phi_\varepsilon^1,\Delta\phi^2]^T[\Delta\phi_\varepsilon^1,\Delta\phi_\varepsilon^2]$ in order for $v_{k_1,k_2}(t)$ to be the ML estimate for the fine resolution at each (k_1,k_2).

$$P = E(\frac{1}{A^2}\begin{bmatrix} m_1^2 - m_o^2 \\ -m_2^2 + m_o^2 \end{bmatrix} \quad [m_1^2 - m_o^2, \ -m_2^2 + m_o^2])$$

$$+ E(\frac{1}{A^2}\begin{bmatrix} w_1^2 - w_o^2 \\ -w_2^2 + w_o^2 \end{bmatrix} \quad [w_1^2 - w_o^2, \ -w_2^2 + w_o^2])$$

$$= (\frac{\sigma_D^2 + \sigma_R^2}{A^2})\begin{bmatrix} 2 + \varepsilon_{11} & -1 + \varepsilon_{12} \\ -1 + \varepsilon_{21} & 2 + \varepsilon_{22} \end{bmatrix}$$

where, $\varepsilon_{i,j}$ is caused by the spatial correlation of $m_i^p(t)$. Let's disregard $\varepsilon_{i,j}$ in P. Then P becomes

$$P = \begin{bmatrix} 2 & -1 \\ -1 & 2 \end{bmatrix} \cdot \frac{(\sigma_D^2 + \sigma_R^2)}{A^2} \quad .$$

Consequently, we don't have to know the variances of σ_D^2 and σ_R^2 as well as $\varepsilon_{i,j}$ in the formula of $v_{k_1,k_2}(t)$. The only knowledge necessary in P is $\begin{bmatrix} 2 & -1 \\ -1 & 2 \end{bmatrix}$ as before. However, it

should be noted that $v_{k_1,k_2}(t)$ is no longer ML estimate now.

All possible set of (k_1,k_2) establishes the set of hypotheses to be tested, given arbitrary lengths of baselines. We will define the effective observable for the ambiguity resolution.

$$v(t) - v_{k_1,k_2}(t) = e(k_1,k_2,t)$$

$$= \sin\theta(t) - (\pi[p,q]P^{-1}\begin{bmatrix} p \\ q \end{bmatrix})^{-1}[p,q]P^{-1}\begin{bmatrix} \Delta\phi_1 + 2\pi k_1 \\ \Delta\phi_2 + 2\pi k_2 \end{bmatrix}$$

$$\gtrdot -(\pi[p,q]P^{-1}\begin{bmatrix} p \\ q \end{bmatrix})^{-1} \cdot [p,q]P^{-1}\begin{bmatrix} \Delta\phi_{\epsilon_1}(t) \\ \Delta\phi_{\epsilon_2}(t) \end{bmatrix} \text{, at the true}$$

hypothesis. (4.50)

Define $z_1^{k_1,k_2}(t) = \Delta\phi_1(t) - p\pi v_{k_1,k_2}(t) + 2\pi k_1$

$$z_2^{k_1,k_2}(t) = \Delta\phi_2(t) - q\pi v_{k_1,k_2}(t) + 2\pi k_2$$

(4.51)

Combination of Eqs. (4.49), (4.50) and (4.51) yields

$$\begin{bmatrix} z_1^{k_1,k_2}(t) \\ z_2^{k_1,k_2}(t) \end{bmatrix} = \begin{bmatrix} q'q, & -pq' \\ -qp', & pp' \end{bmatrix}\begin{bmatrix} \Delta\phi_\epsilon^1(t) \\ \Delta\phi_\epsilon^2(t) \end{bmatrix} \text{ at the true}$$

hypothesis, where

$$[p', q'] = ([p, q]P^{-1}\begin{bmatrix} p \\ q \end{bmatrix})^{-1}[p, q]P^{-1}$$

thus $p'p + q'q = 1$ and $p', q' \geqslant 0$, $p' \neq q'$. The above square matrix is singular as expected. At the true hypothesis,

99

$$z_1^{k_1,k_2}(t) - z_2^{k_1,k_2}(t) = (p' + q') \, [q, \, -p] \begin{bmatrix} \Delta\phi_\epsilon^1(t) \\ \Delta\phi_\epsilon^2(t) \end{bmatrix}$$

"–" sign is taken for example. Hence, define final effective observable $z(k_1,k_2,t)$ for the ambiguity resolution by,

$$z(k_1,k_2,t) = \frac{1}{p' + q'} (z_1^{k_1,k_2}(t) - z_2^{k_1,k_2}(t)) \qquad (4.52)$$

$$\rightarrow [q, \, -p] \begin{bmatrix} \Delta\phi_\epsilon^1(t) \\ \Delta\phi_\epsilon^2(t) \end{bmatrix} \text{ at the true hypothesis.}$$

Let the true hypothesis be (j_1,j_2) explicitly from now on.

$$z_1^{k_1,k_2}(t) = \Delta\phi_1(t) - p[p', \, q'] \begin{bmatrix} \Delta\phi_1 + 2\pi k_1 \\ \Delta\phi_2 + 2\pi k_2 \end{bmatrix} + 2\pi k_1$$

$$= z_1^{j_1,j_2}(t) - p[p',q'] \begin{bmatrix} k_1 & -j_1 \\ k_2 & -j_2 \end{bmatrix} \cdot 2\pi + 2\pi(k_1 - j_1)$$

$$z_2^{k_1,k_2}(t) = z_2^{j_1 \cdot j_2}(t) - q[p',q'] \begin{bmatrix} k_1 & -j_1 \\ k_2 & -j_2 \end{bmatrix} \cdot 2\pi + 2\pi(k_2 - j_2).$$

Thus $z(k_1,k_2,t) = z(j_1,j_2,t) + \Delta(k_1,k_2)$ $\qquad (4.53)$

with $z(j_1,j_2) = [q, \, -p] \begin{bmatrix} \Delta\phi_\epsilon^1 \\ \Delta\phi_\epsilon^2 \end{bmatrix}$ and,

$$\Delta(k_1,k_2) = 2\pi[q(k_1 - j_1) - p(k_2 - j_2)]. \qquad (4.54)$$

When p and q are coprime and also $p,q = $ (even$\leftrightarrow$odd), $\Delta(k_1,k_2) = $

100

0 if any only if $(k_1, k_2) = (j_1, j_2)$ for any (k_1, k_2) of interest. As a note, the additional condition that $(p,q) =$ (even↔odd) is necessary to avoid the ambiguity at extreme hypotheses, (e.g. in Fig. 3.7; $(-2, -2)$, $(1,1)$ the extreme ones) when one of them is true.

Hence $z(k_1, k_2, t)$ is a gaussian process with mean $\Delta(k_1, k_2)$ at a false hypothesis, and becomes a gaussian with mean zero at the true hypothesis. Thus the sequential test reduces to the sequential mean test, particularly with $z(j_1, j_2, t)$ being shared among all $z(k_1, k_2, t)$.

Define $\lambda(k_1, k_2, T_p)$ for each hypothesis $H(k_1, k_2)$ as below.

$$\lambda(k_1, k_2, T_p) = \log p(z(0), z(1), \ldots, z(T_p - 1))$$

$$\begin{bmatrix} p & \text{is joint pdf.} \\ z(t) & \text{is defined under each } H(k_1, k_2) \end{bmatrix}$$

$$= \sum_{t=0}^{T_p - 1} \log p(z(t)), \text{ due to whiteness of } z(\cdot).$$

But,

$$p(z(t)) = \frac{1}{\sqrt{2\pi}\ \sigma_t} \exp\left(-\frac{1}{2\sigma_t^2} z^2(t)\right)$$

where

$$\sigma_t = [q, -p] \cdot P_o \cdot \begin{bmatrix} q \\ -p \end{bmatrix}$$

$$P_o = E[\Delta\phi_\varepsilon^1, \Delta\phi_\varepsilon^2]^T [\Delta\phi_\varepsilon^1, \Delta\phi_\varepsilon^2].$$

Thus

$$\lambda(k_1, k_2, T_p) = \sum_{t=0}^{T_p-1} \log\left(\frac{1}{\sqrt{2\pi}\,\sigma_t}\right) - \frac{1}{2\sigma_t^2} \sum_{t=0}^{T_p-1} z^2(k_1, k_2, t)$$

(4.55)

Maximizing $\lambda(k_1, k_2, T_p)$ is equivalent to minimizing

$y(k_1, k_2, T_p) = \sum_{0}^{T_p-1} z^2(k_1, k_2, t)$, and under the assumption of

local stationarity we don't have to know the underlying

covariance matrix P_o. The ambiguity resolution is achieved

by selecting (j_1, j_2) that minimizes $y(k_1, k_2, T_p)$ over (k_1, k_2).

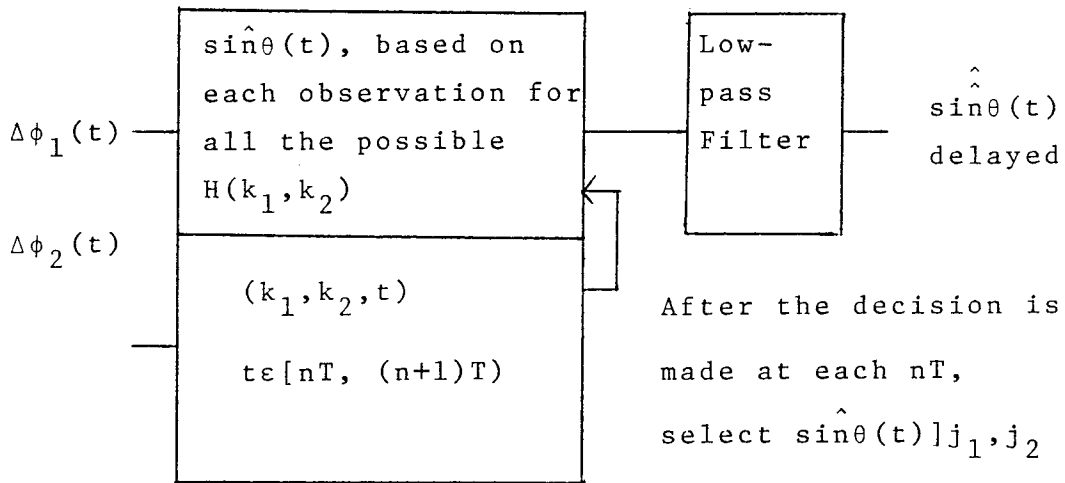Implementation of these combined algorithms can be

depicted by Fig. 4.12.

Fig. 4.12. Implementation of algorithm.

At the true hypothesis, $\sin \hat{\theta} (t)$ is given from Eq. (4.50) by,

$$\sin \hat{\theta}(t) = \sin\theta(t) + [\pi[p, q]P^{-1} \begin{bmatrix} p \\ q \end{bmatrix}]^{-1}[p,q]P^{-1} \begin{bmatrix} \Delta\phi_\varepsilon^1(t) \\ \Delta\phi_\varepsilon^2(t) \end{bmatrix}$$

Los pass filter smoothes the estimation error (caused by $\Delta\phi_\varepsilon^1(t)$, $\Delta\phi_\varepsilon^2(t)$) by rejecting the fluctuating high-frequency portion. Consequently, although $\sin \hat{\theta}(t)$ is not ML estimate, these estimates are improved by the filtering to a certain extent. When the number of the ambiguity lobes is quite a lot, the following version can be useful.

(1) In the search mode of interferometer, use the usual statistic based on each observation described in Section 3.3.

(2) After the reliable acquisition is made, say (j_1, j_2), use the sequential hypothesis test on the neighboring set of hypotheses around (j_1, j_2). Update (j_1, j_2) continuously as the decisions are made.

5. CONCLUSION

Comparison and future area

In the derivation of statistic for estimating the source direction, the statistics of observables usually does not include the effect of scattering from the rough surface. That is, the source-dependent noises are not considered. Also the statistic is usually based on each observation, so that the first order distribution is all the statistical knowledge required. Accordingly the statistic is usually simple, but is more susceptible to a performance degradation in the multipath environment. In Cases II and III of Chapter 3, a knowledge of covariance matrix of noise is not necessary to estimate the source direction, as far as the observed noises are spatially independent and identical, and are independent of $\vec{\mu}$ assumed. In Case IV, only the variance of receiver noise is required to obtain the sampled covariance matrix of source signals.

In this thesis, we have considered the linear horizontal interferometer under the multipath environment. Our work has been carried out in a way to use the observations sequentially and to include the background noise statistics, due to the scattering from rough surface. The sequential maximum likelihood estimator has been derived, and applied to the local interval of μ_1. Consequently a computational complexity is reduced, due to the tracking version. We have assumed one source under the homogeneous rough surface in the derivation of algorithm. Measurements

of some underlying parameters are necessary to implement

the proposed algorithm, due to its consideration of the

multipath effect. We also have extended the statistic in

Section 3.3 to the combined form, in which measurements of

the underlying parameters are not necessary due to the

assumptions in Section 4.7.

The essential assumptions are as follows: Firstly,

we have assumed that emitter is stationary in the cell of

interest during several multiples of processing period T_p.

Secondly, the models of random processes involved remain

as a problem to be examined further.

The future goal is to make the sequential algorithm

an adaptive one, which ensures the adaptive convergence

of the estimate in a multiple source situation under the

environment of rough surface.

REFERENCES

[1] Petr Beckmann and André Spichizzino, "The scattering of electromagnetic waves from rough surfaces," Chapters 5, 12. Pergamon Press, 1963.

[2] C.I. Beard, "Coherent and incoherent scattering of microwaves from the ocean," IRE Transactions on Antennas and Propagations, Vol. Ap-9, (Sept. 1961), pp. 470-483.

[3] F.G. Bass and I.M. Fuks, "Wave Scattering from Statistically Rough Surfaces," Chapter 7. Pergamon Press, 1979.

[4] C.I. Beard and I. Katz, "The dependence of microwave radio signal spectra on ocean roughness and wave spectra," IRE Transactions on Antennas and Propagation, Vol. AP-5 (April 1957), pp. 183-191.

[5] H.L. Van Trees, "Detection, Estimation, Modulation Theory," Part I. New York, Wiley, 1968.

[6] I.N. El-Behery and R.H. Macphie, "Radio source parameter estimation by maximum likelihood processing of variable baseline correlation interferometer data," IEEE Transactions on Antennas and Propagation, Vol. AP-24, (March 1976), pp. 163-173.

[7] T.P. Mcgarty, "The effect of interfering signals on the performance of angle of arrival estimates," IEEE Transactions on Aerospace and Electronic systems, Vol. AES-10, No. 1, (Jan. 1974), pp. 70-77.

[8] T. Kailath, "Correlation detection of signals perturbed by a random channel," IEEE Transactions on Information Theory (June 1960), pp. 361-366.

[9] N. Malloy, "Effect of quantization on gross error probability in three element linear interferometers," Litton Amecon, Office correspondence, April 1981.

[10] S.S. Reddi, "Multiple source location - a digital approach," IEEE Transactions on Aerospace and Electronic Systems, Vol. AES-15, No. 1, (Jan. 1979), pp. 95-105.

[11] I.N. El-Behery and R.H. Macphie, "Maximum likelihood estimation of the number, directions, strengths of point radio sources from variable baseline interferometer data," IEEE Transactions on Antennas and Propagation, Vol. AP-26, No. 2, (March 1978), pp. 294-301.

[12] T.P. Mcgarty, "Antenna performance in the presence of diffuse multipath," IEEE Transactions on Aerospace and Electronic Systems, Vol. AES-12, No. 1 (Jan. 1976), pp. 42-54.

[13] D.E. Barrick, "Rough surface scattering based on the specular point theory," IEEE Transactions on Antennas and Propagation, Vol. AP-16, No. 4 (July 1968), pp. 449-454.

[14] K.M. Mitzner, "Change in polarization on reflection from a tilted plane," Radio Science, Vol. 1 (Jan. 1966), pp. 27-29.

[15] R.J. Wagner, "Shadowing of randomly rough surface," The Journal of the Acoustical Society of America, Vol. 41 (1967), pp. 138-147.

[16] Fred C. Schweppe, "Evaluation of likelihood functions for gaussian signals," IEEE Transactions on Information Theory (Jan. 1965), pp. 61-70.

[17] T.P. Mcgarty, "Azimuth-elevation estimation performance of a spatially dispersive channel," IEEE Transactions on Aerospace and Electronic Systems, Vol. AES-10, No. 1, January 1974.